UNIVERSITY OF CALIFORNIA
RIVERSIDE

Assessment of Skeletal Malformations Associated With Embryonic Toxicant Exposure

A Thesis submitted in partial satisfaction
of the requirements for the degree of

Master of Science

in

Environmental Toxicology

by

Madeline Karen Marie Vera-Colon

September 2022

Thesis for Committee:
Dr. Nicole zur Nieden, Chairperson
Dr. David Volz
Dr. Sihem Cheloufi

The Thesis of Madeline Karen Marie Vera-Colon is approved:

_____

_____

_____

Committee Chairperson

University of California, Riverside

ACKNOWLEDGEMENTS

I have been blessed with many supportive people that have helped push me to achieve this accomplishment.

I would like to acknowledge my thesis advisor Dr. Nicole I. zur Nieden and thank her for providing me with an environment where I was able to accomplish so much.

The preliminary work presented here was accomplished by Nicole R.L. Sparks (osteoEST development and tobacco RNA-sequencing samples), Lauren M. Walker (mouse work), Joseph V. Madrid (ToxPI), and Desiree Williams (prior RNA-sequencing work). For some of the work presented here I had assistance from Danielle Zamora (screening dose-responses, mouse measurements), Ruthia Soh (mouse measurements), and Chris Gatdula (mouse measurements). Thank you to all my lab mates. Dr. Nicole Sparks, Ariana Hardy, and Ruthia Soh, you all gave me all my best memories during graduate school, and I will forever be grateful.

Thank you to the Environmental Toxicology graduate program and my thesis committee members Dr. David Volz and Dr. Sihem Cheloufi. You both provided me with vital feedback and support in graduate school and for that I am thankful. Thank you to the Environmental Toxicology graduate program director, Dr. Wenwan Zhong and graduate advisor, Dr. Quan Cheng for their prompt and vital support during my time at UCR. A thank you to Antonio Knox and Fidel Rivas for helping me navigate the logistical side of graduate school. I would like to thank Dr. Prue Talbot (University of California, Riverside) for providing our lab with the Camel Blue sidestream tobacco smoke solutions used for Chapter 3 and 5 of this work.

To my greatest friends, Ariana, Tess, and Terry, thank you for helping me stay sane over the years; I am so happy to have met you along this journey. To my favorite people on Earth, my little sisters, Mikaela and Gracie Vera: I love you both with my whole heart. To my parents, Raul and Melissa Vera, everything I do is to make the both of you proud. Thank you for your sacrifices.

To the one I owe everything to, my husband Katsuya Colon: thank you for always believing in me even when I did not believe in myself. I love you and to our two cat sons, Myelin and Helix Vera-Colon thank you for the endless snuggles. Without you three, this could not have been possible.

ABSTRACT OF THE THESIS

Assessment of Skeletal Malformations Associated With Embryonic Toxicant Exposure

by

Madeline Karen Marie Vera- Colon

Master of Science, Environmental Toxicology
University of California, Riverside, September 2022
Dr. Nicole zur Nieden, Chairperson

Tobacco use during pregnancy poses many risks to reproductive health and unborn life. Children exposed to tobacco *in utero* grow up to experience abnormalities ranging from cognitive or developmental deficits to malformations of the skeleton, such as cleft lip and palate, as well as an increased risk of fractures following minor injuries. While numerous studies demonstrate the adverse effects of tobacco-related products towards human health and developing embryos, the molecular underpinnings of embryonic skeletal maldevelopment remain unclear largely due to the inadequacy of existing model systems. Moreover, new tobacco products are being introduced into the market, despite fervent public health initiatives. One such product is Snus, a non-combustible chewing type of tobacco. Snus received clearance to be advertised as a harm-reduction product, and hence would be an attractive alternative to pregnant smokers unable to quit. Yet here we provide evidence that Snus might not be free of all harm. Our lab has previously found a robust and reproducible hypomineralized phenotype in multiple bones of mice and zebrafish when exposed to smoke extracts of Snus tobacco during development. This phenotype of reduced

calcification can also be detected when human embryonic stem cells (hESCs) are exposed during differentiation to bone-forming osteoblasts, thereby providing an adequate human *in vitro* model to study tobacco-exposure-mediated hypomineralization.

This hESC model will serve as the primary relevancy to human health to expose the negative implications of tobacco, primarily Snus, on prenatal bone health and work to negate the changes in the osteogenic molecular framework caused by Snus tobacco exposure. By extension, new insight on the molecular mechanism of tobacco-induced hypomineralization has implications beyond tobacco exposure. This work could provide a solid framework for future analyses of human genetic traits that increase the risk for congenital skeletal diseases. As a result, new guidelines could be implemented by the American Academy of Pediatrics for pediatricians to conduct well-childcare exams in which pre-visit questionnaires include questions on the type of tobacco the child was/is exposed to. After exposure is confirmed, bone health and quality should be routinely assessed, appropriate parental education executed, and fracture prevention strategies discussed with the family.

TABLE OF CONTENTS

LIST OF FIGURES

LIST OF TABLES

CHAPTER 1: EVOLUTION OF STEM CELL RESEARCH & EVALUATION OF HUMAN EMBRYONIC STEM CELLS AS A MEANS OF RECAPITULATING EMBRYONIC DEVELOPMENT

1. Introduction

1.1 Stem Cell Properties

Stem cell utilization is infinite and remains at the forefront of cutting-edge research. There are many sources in which stem cells can originate, yet all stem cells have the capability of self-renewal while maintained in an undifferentiated state (He et al., 2009). As such, stem cells make excellent candidates for cell regeneration studies (Mahla et al., 2016). However, stem cell research is pivoting to take advantage of the seemingly limitless differentiation capabilities. Embryonic stem cells (ESCs) are pluripotent, and therefore can differentiate into any specialized cell types of the body that are derived from the three primary germ layers, such as neurons, skin cells, and bone cells **(Figure 1.1**). With the use of stem cell differentiation, ESCs can be used to recapitulate embryonic development and asses the effects of environmental exposure on embryogenesis.

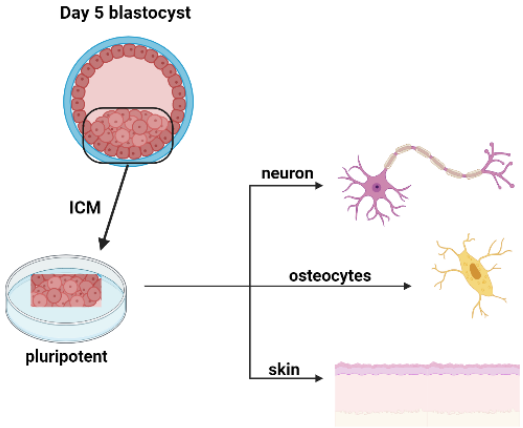

Figure 1.1 Isolated pluripotent ESCs from the inner cell mass of a day 5 human blastocyst. Created with Biorender.

Stem Cell Types. Adult stem cells (ASCs) are derived from somatic tissues, such as bone marrow or fat, that are limited to differentiating into cell types specific to the tissues or organs in which they live. Due to the limited differentiation capacity of ASCs, they have multi- or uni-potent potential (Dulak et al., 2015). Also, ASCs can only undergo a limited number of divisions. ASCs, therefore, mostly contribute to tissue homeostasis and thus ultimately are responsible for tissue repair, especially in areas of the body that undergo high turnover (Pekovic et al., 2008).

Unlike ASCs, ESCs are unspecialized cells that have high self-renewal properties and can be maintained in a pluripotent state. Pluripotency allows ESCs to give rise to any cell type derived from the three germ layers (Keller et al., 2005) (**Figure 1.2**). ESCs are derived from the inner cell mass of the blastocyst (Martin et al., 1981; Evans and Kauffman, 1981). In vivo, it is the inner cell mass of the blastocyst that becomes the embryo proper, thus ESCs are unable to give rise to extraembryonic tissues and therefore cannot create an organism. Despite the undeniable utility of stem cells, first reports only surfaced in the early 1980s of ESCs isolated from mice (Martin et al., 1981; Evans & Kaufman, 1981).

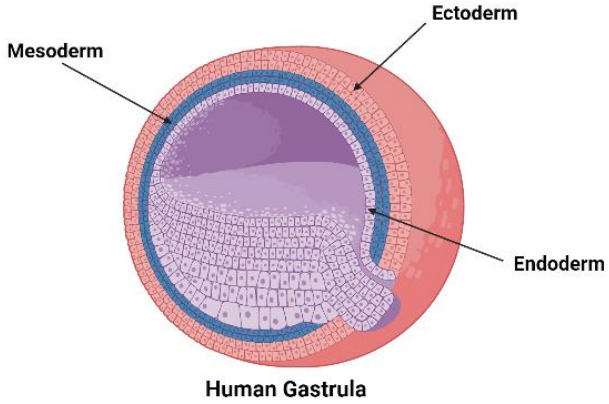

Figure 1.2 A human gastrula depicting the primary germ layers, which will later help form the notochord, neural tube, and somite after gastrulation. Created with Biorender.

The use of mouse ESCs (mESCs) outlined truly remarkable work and allowed for the advancement of both culture techniques and other exploratory ESC work. As such, mESC work paved the way for the derivation of human ESCs (hESCs) from cryopreserved blastocysts in the late 1990s (Thomson et al., 1998).

While in culture hESCs, like mESCS, can be maintained in an undifferentiated state. However, researchers are able to manipulate spontaneous differentiation depending on cell maintenance and passaging protocols. Directed ESC differentiation into specified cell types is facilitated through changes in culture medium that inhibit pluripotency and promote upregulation of lineage-specific gene. Many ESC differentiation protocols that have been reported, including differentiation into cardiomyocytes, neurons, and also bone-forming osteoblasts (Okabe et al., 1996; zur Nieden et al., 2003; zur Nieden et al., 2005). As ESCs decrease in pluripotency and differentiate towards a specific lineage, they progress through several progenitor cell fates before becoming a differentiated cell type, such as an osteoblast (**Figure 1.3**).

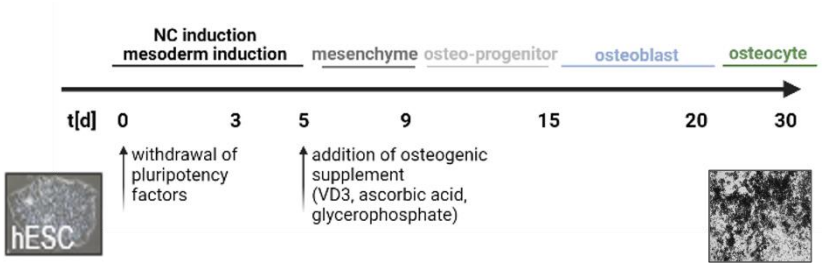

Figure 1.3. Cellular stages of human embryonic stem cells as undergo osteogenesis. Created with Biorender

1.2 Bone Development

Osteogenesis. Osteogenesis is defined as the formation and development of bones. The skeleton arises from three distinct lineages. Neural crest cells migrate to form most of the

craniofacial skeleton and cartilage (Knight and Schilling, 2000). The somites, which originate from the mesoderm, form the axial skeleton, the ribs and vertebrae (Kageyama et al., 2010), and the lateral plate mesoderm forms the appendicular skeleton (Tani et al., 2020). Together these distinct pre-skeletal lineages make up the skeletal components described below.

Skeletal Components. Bone is composed of compact tissue and cancellous tissue, which is maintained by osteoblasts, the bone-forming, and osteoclasts, the bone-resorbing cells. Both specialized cell types are constantly being turned over throughout life in a process called bone remodeling. Osteoblasts synthesize the bone matrix and promote mineralization of the extracellular matrix. Derived from hematopoietic precursors, multi-nucleated osteoclasts form resorption pits on the bone surface and degrade the bone matrix proteins by the use of enzymes, such as Cathepsin K (Touaitahuate et al., 2014). The third component of a long bone are the chondrocytes which are the only cells found in healthy cartilage. They produce and maintain the cartilaginous matrix, which consists mostly of collagen and proteoglycans (Akkiraju and Nohe, 2015). Chondrocytes help regulate the bone extracellular matrix and maintain cartilage homeostasis (Akkiraju and Nohe, 2015).

Skeletogenic bone formation can occur through endochondral ossification, which includes an intermittent cartilage phase, or directly through osteoblast formation in intramembranous ossification. Endochondral ossification outlines the formation of all the bones in the body, except the flat bones, clavicles, and mandible and is also responsible for fracture healing in adults. Both endochondral ossification and intramembranous ossification arise from a group of mesenchymal cells. In areas of endochondral ossification,

condensed mesenchymal cells differentiate into chondrocytes to form a cartilage template for the future bony skeleton. During intramembranous ossification, mesenchymal cells condense and directly convert into osteoblasts, creating the flat bones. Regardless of lineage derivation, once the osteoblast becomes buried in the mineralized bone, it will mature into an osteocyte. Whereby, osteoblasts work to continue producing new bone cells and osteocytes contribute to bone mass.

Developmental Disorders of the Bone. There are numerous skeletal disorders that can arise due to defects in skeletal patterning, differentiation, growth, and/or homeostasis. Some forms of skeletal dysplasia are fatal; however, many are not. Exposure to several toxicants during embryonic development can result in a plethora of birth defects, such as exposure to cyclopamine during early embryogenesis prevents the brain from forming two lobes and when not fatal can result in the formation of a single eye (Heretsch et al., 2010). Distinct skeletal disorders such as thanatophoric dysplasia, campomelic dysplasia, achondroplasia, osteogenesis imperfecta, and achondrogenesis can be caused by exposure to a toxicant as skeletal development takes place (chop.edu/conditions-diseases/skeletal-dysplasias). Although screening of parents can give some insight into genetically inherited skeletal disorders, they can also arise from spontaneous mutations or secondary exposure without prior family history.

In Vitro Osteogenesis. Osteoblast differentiation is a complex process controlled by stage specific regulatory genes. *In vitro,* bone differentiation from mESCs was first assessed by zur Nieden et al. (2003) using murine ESCs and osteogenesis factors ascorbic acid, β-glycerophosphate and 1,25-$(OH)_2$ vitamin D_3. The current physical assessment of *in vitro*

osteogenesis includes identifying bone-forming cells in culture. Their presence is evident by the manifestation of a calcified extracellular matrix, which is a hallmark of bone cells and provides the characteristic strength to the bone tissue. The osteoblast differentiation protocol remains an effective way of producing these bone-forming cells in a process that follows the *in vivo* stages of embryonic development outlined above. In the first four days of this differentiation protocol, cells exit from pluripotency and undergo spontaneous differentiation whereby the three germ layers are stochastically represented. On Day 5, three supplements are added to the base medium, which are ascorbic acid, beta-glycerophosphate, and the bone active factor, $1\alpha,25\text{-}(OH)_2$ vitamin D_3 which enhances the differentiation and mineralization of mature osteoblasts (**Figure 1.3**). Beta-glycerophosphate provides cells with a source of inorganic phosphate and is the substrate for *alkaline phosphatase* (*ALP*) (zur Nieden., 2011), which is a major enzyme involved in mineralization and early marker of osteoblast differentiation (zur Nieden., 2011). In osteoblast-precursors and early osteoblast stages the transcription factor, *runt-related transcription factor 2* (*RUNX2*) is highly expressed (Ducy et al., 1997) and is required for osteoblast differentiation. *RUNX2* regulates the expression of osteogenic genes, including *osteopontin* and mature osteoblast markers *osteocalcin* (*OCN*) and *bone sialoprotein* (*BSP*) (Ducy et al., 1997; Nakashima et al., 2002). Molecular alteration at any point during osteogenesis can result in a skeletal defect (zur Nieden et al., 2010).

This protocol remains over 90% efficient in osteoblast differentiation and is highly reproducible across species (zur Nieden et al., 2004; zur Nieden et al., 2003; zur Nieden et al., 2007; Kuske et al., 2011; zur Nieden et al., 2005). In rhesus, common marmoset and

human ESCs and induced pluripotent stem cells (iPSCs), vitamin D_3 supplementation equally leads to the commitment of bone lineage cells accompanied by characteristic gene expression and ending with a calcified extracellular matrix that appears black in phase contrast microscopy (Dienelt et al., 2010; Trettner et al., 2014; Sparks et al., 2018).

1.3 Embryonic Stem Cell Test (EST)

The 1960's global thalidomide disaster higlighted the negative effects of chemical and environmental toxicant insults on embryotoxicity. To prevent such adverse effects on developing embryos, chemicals are required to be screened according to OECD guidelines (Lee et al., 2012; Mouche et al., 2011; Spielmann et al., 1997). Such screenings are conducted in live animals, mostly rodents (Lee et al., 2012) and zebrafish embryos which are routinely used as a method for assessing developmental toxicity (Caballero and Candiracci, 2018). However, *in vivo* approaches are time consuming, require a large amount of animals, costly, and lack human-centered risk assesment. In turn, *in vitro* approaches allow for safe, reliable, and high throughput results. Three such approaches based on *in vitro* assays include the micromass whole cell culture assay, the Frog Embryo Teratogenesis Assay-Xenopus (FETAX) test, and the Embryonic Stem Cell Test (EST) (Lee et al., 2012; Mouche et al., 2011; Spielmann et al., 1997). These techniques were validated in 2002 by the European Centre for Validation of Alternative Methods for accuracy and predictivity. While all three were found useful, only the EST completely avoided the use of animals. In addition to avoiding the sacrificial use of animals, the EST is less labor-intensive than other *in vitro* techniques. The EST classfication of the embryotoxic potenital of a test compound uses three endponts: cytotoxicity of 1) 3T3

mouse adult cells and (2) ESCs (the test compound's concentration resulting in a 50% decrease in cell viability, IC_{50}) and (3) inhibition of differentiation of ESCs (the test compound's concentration that results in 50% cardiomyocyte differenitation inhibition, ID_{50}) (Scholz et al., 1999; Genschow et al., 2004; Genshow et al., 2002). In the classic EST invented by Spielmann and colleagues, evaluation of differentiation inhibition is based on the absence or presence of contracting cardiomyocyte clusters in a stem cell culture as an indicator of embryotoxicity. Dose response curves determine IC_{50} and ID_{50} values, which are then incorporated into a bio-statistical model, where chemicals are predictively classified into one of three embryotoxic categories: strongly embryotoxic, weakly embryotoxic, and non-embryotoxic (Genschow et al., 2002). Follow-up validation studies found the EST had a 78% correct classification for the tested compounds and 100% predictive in cateogorizing stong embryotoxicants. However, this method was limited to one differentiation endpoint and cannot be used to predict other teratogenicities.

zur Nieden et al. first expanded the mouse-based EST to contain a skeletal endpoint (2004). However, current experimental assessments of rodent responses extrapolated to human exposure are unable to predict accurate gestational development and exposure on humans. While a rigorously controlled experiment with the above-mentioned method may uncover a causal relationship between exposure and skeletal birth defects, *in vivo* work remains labor- and cost-intensive and require sacrificing pregnant animals to recover embryos. With the advent of human pluripotent stem cell models and their application to derive bone cells, it has now become possible to leverage these cells for risk assessment associated with environmental exposure.

By employing human embryonic stem cells to this embryotoxicity model, the zur Nieden lab has remained at the forefront of improving the EST. Similar to the classic EST, this hEST also utilizes three endpoints: cytotoxicity of (1) human foreskin fibroblasts (hFF, adult cells), (2) human ESCs and (3) differentiation of hESCs into osteoblasts. In prior studies in the lab, osteoblast differentiation was assessed by the indirect measurement of calcium deposition (ID_{50}Ca) and *TWIST1* gene expression (ID_{50}*TWIST1*). Through comparison with results obtained with the mEST on a small battery of test chemicals with known *in vivo* embryotoxicity potential, the suitability of this modified EST using human ESCs was demonstrated. In particular, 13-cis retinoic acid, which is embryotoxic to the human skeleton, but not the mouse (Nau, H. 2001), was classified as a moderately embryotoxic chemical. Therefore, the modified hEST was able to correlate developmental toxicity to certain environmental toxicants and assess skeletal birth defects.

References

1. Akkiraju, H & Nohe, A. 2015. Role of Chondrocytes in Cartilage Formation, Progression of Osteoarthritis and Cartilage Regeneration. *J Dev Biol.* 3(4): 177–192. doi:10.3390/jdb3040177.

2. Caballero MV, Candiracci M. 2018. Zebrafish as screening model for detecting toxicity and drugs efficacy. *J Unexplored Med Data* 3:4. http://dx.doi.org/10.20517/2572-8180.2017.15

3. Davis, L.A., and zur Nieden, N.I. 2008. Mesodermal fate decisions of a stem cell: the Wnt switch. *Cell. Mol. Life Sci.* 65(17), 2658–2674.

4. Ducy, P., Zhang, R., Geoffroy, V., Ridall, A.L., and Karsenty, G. 1997. Osf2/Cbfa1: a transcriptional activator of osteoblast differentiation. *Cell* 89(5), 747–754.

5. Dulak J, Szade K, Szade A, Nowak W, Józkowicz 2015. A. Adult stem cells: hopes and hypes of regenerative medicine. *Acta Biochim Pol.* 62(3):329-37. doi: 10.18388/abp.2015_1023. Epub 2015 Jul 22. PMID: 26200199.

6. Evans MJ, Kaufman MH. 1981. Establishment in culture of pluripotential cells from mouse embryos. *Nature.* 292(5819):154-6.

7. Genschow E; Spielmann, H; Scholz, G; Seiler, A; Brown, N; Piersma, A; Brady, M; Clemann, N; Huuskonen, H; Paillard, F; Bremer, S; Becker, K. 2002. The ECVAM international validation study on *in vitro* embryotoxicity tests: results of the definitive phase and evaluation of prediction models. Altern. Lab Anim. 30(2):151-76.

8. Genschow E, Spielmann H, Scholz G, Pohl I, Seiler A, Clemann N, Bremer S, Becker K (2004). Validation of the embryonic stem cell test in the international ECVAM validation study on three *in vitro* embryotoxicity tests. Altern Lab Anim. 32(3):209-44.

9. He S, Nakada D, Morrison SJ. 2009. Mechanisms of stem cell self-renewal. *Annu Rev Cell Dev Biol.* 25:377-406. doi: 10.1146/annurev.cellbio.042308.113248.

10. Heretsch P, Tzagkaroulaki L, Giannis A. 2010. Cyclopamine and hedgehog signaling: chemistry, biology, medical perspectives. *Angewandte Chemie.* 49 (20): 3418–27. doi:10.1002/anie.200906967. PMID 20429080.

11. Kageyama, R., Niwa, Y., Shimojo, H., Kobayashi, T., Ohtsuka, T. 2010. Ultradian oscillations in Notch signaling regulate dynamic biological events. *Curr. Top. Dev. Biol.*, (92)311-331, 10.1016/S0070-2153(10)92010-3

12. Keller, G. 2005. Embryonic stem cell differentiation: emergence of a new era in biology and medicine. *Genes & Dev.* 19: 1129-1155

13. Knight RD, Schilling TF. 2000. Cranial Neural Crest and Development of the Head Skeleton. In: Madame Curie Bioscience Database. *Landes Bioscience*

14. Kuske B, Savkovic V, zur Nieden NI. 2011. Improved media compositions for the differentiation of embryonic stem cells into osteoblasts and chondrocytes. *Methods* Mol Biol. 690:195-215.

15. Lee HY, Inselman AL, Kanungo J, Hansen DK. 2012. Alternative models in developmental toxicology. *Syst Biol Reprod Med.* 58(1):10-22.

16. Mahla, RS. 2016. Stem cells applications in regenerative medicine and disease therapeutics. *International Journal of Cell Biology.* (5):e6940283. doi: 10.1155/2016/6940283.

17. Martin GR. 1981. Isolation of a pluripotent cell line from early mouse embryos cultured in medium conditioned by teratocarcinoma stem cells. *Proc Natl Acad Sci USA*. 78(12):7634-8.

18. Metzger, J. M., W.-I. Lin, R. A. Johnston, M. V. Westfall, and L. C. Samuelson. 1995. Myosin Heavy Chain Expression in Contracting Myocytes Isolated During Embryonic Stem Cell Cardiogenesis. *Circulation Research* 76(5): 710-19.

19. Mouche I, Malesic L, Gillardeaux O. 2011. FETAX assay for evaluation of developmental toxicity. *Methods Mol. Biol.* 691: 257-269.

20. Nakashima, K., Zhou, X., Kunkel, G., Zhang, Z., Deng, J.M., Behringer, R.R. 2002. The novel zinc finger-containing transcription factor osterix is required for osteoblast differentiation and bone formation. *Cell* 108, 17–29.

21. Nau, H. 2001. Teratogenicity of isotretinoin revisited: Species variation and the role of all-trans-retinoic acid. *JAAD* 45(5), S183-S187.

22. Okabe S, Forsberg-Nilsson K, Spiro AC, Segal M, McKay RD. 1996. Development of neuronal precursor cells and functional postmitotic neurons from embryonic stem cells *in vitro*. *Mech Dev.* 59(1):89-102.

23. Pekovic, V., & Hutchison, C. J. 2008. Adult stem cell maintenance and tissue regeneration in the ageing context: the role for A-type lamins as intrinsic modulators of ageing in adult stem cells and their niches. *Journal of anatomy*. 213(1), 5–25. https://doi.org/10.1111/j.1469-7580.2008.00928.x

24. Scholz G, Genschow E, Pohl I, Bremer S, Paparella M, Raabe H, Southee J, Spielmann H (1999). Prevalidation of the Embryonic Stem Cell Test (EST)-A New *In Vitro* Embryotoxicity Test. Toxicol *In Vitro.* 13(4-5):675-81.

25. Sparks NRL, Martinez IKC, Soto C, zur Nieden NI. 2018. Low osteogenic yield pluripotent stem cells associates with differential neural crest promoter methylation. *Stem Cells.* doi:10.1002/stem.2746

26. Spielmann H, Pohl I, Doring B, Liebsch m, Moldenbauer F. 1997. The embryonic stem cell test (EST), an *in vitro* embryotoxicity test using two permanent cell lines: 3T3 fibroblasts and embryonic stem cells. *In Vitro* Toxicology. 10:119–27.

27. Tani, S., Chung, Ui., Ohba, S. 2020. Understanding paraxial mesoderm development and sclerotome specification for skeletal repair. *Exp Mol Med* 52, 1166–1177. https://doi.org/10.1038/s12276-020-0482-1

28. Thomson JA, Itskovitz-Eldor J, Shapiro SS, Waknitz MA, Swiergiel JJ, Marshall VS Jones JM. 1998. Embryonic stem cell lines derived from human blastocysts. *Science.* 5391(282):1145-1147.

29. Touaitahuata, H., Blangy, A., Vives, V. 2014. Modulation of osteoclast differentiation and bone resorption by Rho GTPases. *Small GTPases.* 5:e28119.

30. Trettner S, Findeisen A, Taube S, Horn PA, Sasaki E, zur Nieden NI. 2014. Osteogenic induction from marmoset ESCs cultured in feeder-dependent and feeder-independent conditions. Osteoporos Int. 25(4):1255-66.

31. Zhang, W.; Sui, Y.; Ni, J; Yang, T. 2016. Insights into the Nanog Gene: A Propeller for Stemness in Primitive Stem Cells. *International Journal of Biological Sciences* 12(11): 1372–1381.

32. zur Nieden NI, Ruf LJ, Kempka G, Hildebrand H, Ahr HJ. 2001. Molecular markers in embryonic stem cells. *Toxicol in vitro* 15:455-61

33. zur Nieden NI, Kempka G, Ahr HJ. 2003. *In vitro* differentiation of embryonic stem cells into mineralized osteoblasts. *Differentiation*. 71(1):18-27.

34. zur Nieden, NI; Kempka, G; Ahr HJ. 2004. Molecular multiple endpoint embryonic stem cell test--a possible approach to test for the teratogenic potential of compounds. *Toxicol. Appl. Pharmacol.* 194(3):257-69.

35. zur Nieden NI, Kempka G, Rancourt DE, Ahr HJ. 2005. Induction of chondro-, osteo- and adipogenesis in embryonic stem cells by bone morphogenetic protein-2: effect of cofactors on differentiating lineages. *BMC Developmental Biology.* 5:1.

36. zur Nieden NI, Price FD, Davis LA, Everitt RE, Rancourt DE. 2007. Gene profiling on mixed ESC populations reveals a biphasic role for beta-catenin in osteogenic differentiation. *Mol Endocrinol* 21:674-685.

37. zur Nieden, NI (ed.), Embryonic Stem Cell Therapy for Osteo-Degenerative Diseases, *Methods in Molecular Biology,* 690, DOI 10.1007/978-1-60761-962-8_1.

Aims and Objectives

Environmental contaminants, including tobacco products, contain many known embryo-toxicants that disrupt skeletal development. However, there has been a lack of attribution of specific chemicals, or class of embryotoxic chemicals, as a causal factor of a skeletal birth defect. The following aims will provide insight on how certain toxicant exposure can influence components of osteogenesis by addressing four specific aims:

Specific Aim 1: Validate the human embryonic stem cell test (EST) on known developmental toxicants (addressed in chapter 2)

Specific Aim 2: Determine skeletal birth defects associated with *in utero* exposure to tobacco extracts (addressed in chapter 3)

Specific Aim 3: Identify specific effects of prevalent constituents during osteogenic differentiation (addressed in chapter 4)

Specific Aim 4: Evaluate hypomineralization phenotype *in vitro* through signal manipulation (addressed in chapter 5)

CHAPTER 2: EMBRYONIC STEM CELL TEST (EST) VALIDATION ON DEVELOPMENTAL TOXICANTS

2.1 Introduction

As previously outlined, skeletal development is a highly complex process that requires many components such as, differentiation, patterning, and morphogenesis. Any mis-regulations within this controlled process can give rise to a skeletal birth defect. While skeletal defects are typically seen as cosmetic defects, treatments that exist are, at best, remedial. These defects can impact quality of life and occur in 1 out of every 4,000 children born (Orioli et al., 1986). While some skeletal defects are genetically inherited, they can also arise from the exposure to toxic agents. With the validation of the human EST (hEST) model, real policies can be implemented to reduce exposure risk in high environmental contaminant areas and prevent birth defects. This work will help establish and employ a reliable *in vitro* model to predict skeletal embryotoxicity of chemicals found in the environment.

The Environmental Protection Agency (EPA) has established a comprehensive bank of toxicants with known effects to the skeleton *in* vivo. A subset of these chemicals was selected to assess the skeletal embryotoxicity within the hEST model. The initial EST was used in an *in vitro* model where mESCs and adult mouse fibroblasts were exposed to toxicants to assess embryotoxicity and maternal toxicity. As previously outlined, the classic mouse EST evaluated cardiac differentiation inhibition during toxicant exposure, however the EST was expanded to encompass other lineage-specific effects (zur Nieden et al., 2003; Festag et al., 2007; Piersma, 2004). In previous years, standard methods for screening

environmental toxicants consisted of exposure-based assay techniques. These models neglect embryo-toxicity and remain too broad to assess exposure on a targeted system. Even the classic EST remained an unreliable technique as a human predictive model, especially in the weak embryotoxic category where it summons a predictivity of only 70%. In order to decrease the amount of false positive and false negative hits, it is hypothesized that a screening approach utilizing a human *in vitro* differentiation model would provide the most predictive results.

Screening toxicants utilized for this proposed model were selected from the EPA's public ToxCast I library. These chemicals have been previously tested using standard screening techniques and have established toxicity reported (Richard et al., 2016). The EPA's ToxCast I library contains over 4,500 chemicals and has been categorized based on relevance of exposure in the environment. The current list was collected over three phases through quality reviews and rigorous high-throughput screening assay-based methods (EPA, 2022). The two categories of assays utilized were cell-based *in vitro* and biochemical *in vitro* assays. The former was used to determine cellular changes in response to exposure and the latter measured the activity of a biological macromolecule. Over 700 different high-throughput assays were utilized which covered about 300 different signaling pathways.

Therefore, the EPA's established ToxCast I list will provide a subset of toxicants to evaluate within a human model. Endpoints within the hEST will be compared back to the mEST. Importantly, both embryonic stem cell lines used for differentiation will contain the same media components on the same time course. However, hESCs require colony confluency before exposure and mESCs simply require the counting of cells (2,500

cells/well) prior to exposure. In both cell differentiation techniques, exposure is consistent and replenished at every media change and as such recapitulates a consistent, environmentally-relevant exposure. The human *in vitro* differentiation model highlights the species-to-species variability in response the screening chemicals selected and also highlights the necessity of implementing a better human-predictive approach.

2.2 Previous data

Prior work in the zur Nieden lab has reliably established the hEST in pairing with a biostatistical model to classify chemicals based on skeletal toxicity. Whereby chemicals were selected based on neural crest-specific toxicity and compared between a human embryonic stem cells (hESCs) and human induced pluripotent stem cells (hiPSCs) line (Sparks et al., in revision). Endpoint analyses revealed that calcium production in the established hESC differentiating line was impacted more than the hiPSCs. Follow-up osteogenic gene detection and mRNA analysis was able to accurately predict chemical classification within the hEST.

Established Positive/Negative Reference Controls as Affecting Osteogenesis Were Utilized.

European Centre for the Validation of Alternative Methods validated positive and negative reference controls were tested in both mouse and human osteoblast differentiation models. Following endpoint collections, identified half-maximal inhibition values were assessed and categorized based on embryotoxicity (non-, weak, strong) using the established biostatistical predication model outlined in Genschow et al., 2002. Using the human EST model, these previously established reference controls were tested to

determine whether human cell responses more accurately predict tissue defects similar to those seen after human exposure. Penicillin G evaluated at the highest relevant concentration (1,000 ug/mL) elicited no effect to osteogenesis both in our model and within the literature (zur Nieden et al., 2004, Walker et al., 2014). Both 5-Fluorouracil (5-FU) and *all-trans* Retinoic Acid (*at*RA) were determined to affect viability and differentiation in mESCs (zur Nieden et al., 2004). While 5-FU is generally cytotoxic, *at*RA elicited a concentration-dependent toxicity to skeletal cells. A derivative of *at*RA was also assessed. 13*cis*RA is a teratogen in humans (Sparks et al. *in revision*). *13cisRA* induced no response in the mouse ESCs, however elicited a similar effect in human ESCs (**Fig 2.1**). This finding suggests that the hEST-based screening technique more accurately categorizes embryo-toxicants.

	Mouse			Human		
Compound	fibroblast	ESC		fibroblast	ESC	
	IC_{50} cytotoxicity (MTT)	IC_{50} cytotoxicity (MTT)	ID_{50} differentiation inhibition (Ca^{2+})	IC_{50} cytotoxicity (MTT)	IC_{50} cytotoxicity (MTT)	ID_{50} differentiation inhibition (Ca^{2+})
Pen G	>1000	800 ± 10.3	>1000	>1000	>1000	>1000
5FU	0.05	0.022 ± 0.0049	0.04 ± 0.006	0.00039 ± 0.000042	0.00019 ± 0.00003	0.00037 ± 0.00002
*at*RA	2.70	0.00009 ± $6.6x10^{-8}$	0.00042 ± 0.000022	0.07 ± 0.0087	0.093 ± 0.019	0.100 ± 0.0274
*13cis*RA	16.67 ± 1.76	14.0 ± 0.5	14.5 ± 1.732	5.35 ± 0.15	1.047 ± 0.127	1.97 ± 0.058

Biostatistical Model		
Compound	Mouse	Human
PenG	Class I	Class I
5FU	Class III	Class III
*at*RA	Class III	Class III
*13cis*RA	Class I	Class II

Class I: non-embryotoxic
Class II: Weak embryotoxic
Class III: Strong embryotoxic.

Figure 2.1: (A) Previously identified reference controls were tested in mouse and human embryonic stem cells and respective adult fibroblasts. Endpoints determined effects to cytotoxicity and osteogenic differentiation. Results also highlight differential effects to mother (fibroblast) and embryo (ESC). Highlighted in the orange boxes demonstrates the species differences with the same exposure. **(B)** The biostatistical model highlights the human ESC model correctly classified control chemicals according to *in vivo* embryotoxicity with greater sensitivity compared to mouse ESCs.

2.3 Methods

2.3.1 Cell Culture

H9 human embryonic stem cells (hESCs) were cultured on Matrigel (BD Biosciences) treated culture plates in mTeSR 1 medium (Stem Cell Technologies) at 37 °C with 5% CO_2. Colonies were passaged every 3 days using accutase (2–4 min at room temperature) and a cell scraper to displace colonies from the plastic well. D3.6 mouse embryonic stem cells (mESCs) were cultured on Primaria-treated culture plates in ESC maintenance medium (15% FBS (Atlanta Biologicals, screened batches), 1% (v/v) non-essential amino acids, 50 U/mL penicillin, 50 µg/mL streptomycin, and 0.1 mM β-mercaptoethanol) at 37 °C with 5% CO_2. Colonies were passaged every 2 days using 0.25% Trypsin-EDTA (5 min at 37 °C). Human foreskin fibroblasts and 3T3 fibroblasts cells were maintained in hFF media (DMEM, 10% maintenance FBS, 1% (v/v) non-essential amino acids, 50 U/mL penicillin and 50 µg/mL streptomycin) and plated into a 0.1% gelatin-coated plate. Cells were passaged every 3 days using 0.25% Trypsin-EDTA (5 min at 37C).

2.3.2 Osteogenic Differentiation of Embryonic Stem Cells

The differentiation protocol established and used within the zur Nieden lab uses confluent H9 hESCs to induce differentiation through the addition of a control differentiation medium (CDM) composed of DMEM, 15% FBS (Atlanta Biologicals), 1% (v/v) non-essential amino acids, 50 U/mL penicillin, 50 µg/mL streptomycin, and 0.1 mM β-mercaptoethanol. CDM is used for the first five days of differentiation to decrease pluripotency. On day five, CDM was supplemented with $1.2*10^{-7}$ M 1,25α$(OH)_2$ Vitamin D_3 (VD_3; Calbiochem), 0.1 mM β-glycerophosphate, and 20.8 µg/mL ascorbic acid. D3.6

mESCs follow the same osteogenic differentiation protocol, however mESCs do not require colony confluency to begin exposure. Cells are counted using Nexcelom Cellometer and plated at 2,500 cells/well.

2.3.3 Exposure of Additional Supplements to Alter Osteogenic Differentiation

Supplemental chemicals 1,3-Dibromo-5,5-Dimethylhydantoin (Sigma Aldrich, 157902, 98%), 17a-Estradiol (Sigma Aldrich, 57-91-0, 98%), 17a-EthinylEstradiol (Sigma Aldrich, E4876, 98%), 5,5-Diphenylhydantoin (Sigma Aldrich, 57-41-0, 98%), Acetaminophen (Sigma Aldrich, A7085, 99%), Benz(a)anthracene (Santa Cruz, sc-252409, 99%), Chloropyrifos (Sigma Aldrich, 45395, ≤100%), Coumarin (Santa Cruz, sc-205637, 98%), Cyclohexamide (Sigma Aldrich, C4859, 90-100%), Cyclopamine (Sigma Aldrich, PHL82510, ≥95%), DEET (Sigma Aldrich, 134-62-3, ≤100%), Folic acid (Sigma Aldrich; 59-30-3, ≥97%), Norgestrel (Sigma Aldrich, N1250000, ≤100%), Quinoline (Sigma Aldrich, 241571, 98%), Sodium Saccharin hydrate (Sigma Aldrich, 47839, ≤100%), Triadimefon (Sigma Aldrich, 45693, ≤100%), and Triadimenol (Sigma Aldrich, 46138, ≤100%) were delivered throughout the entire duration of differentiation with the appropriate concentration. All chemical stocks were diluted to 100,000 µg/mL using DMSO. Working stocks were diluted down to 10,000 µg/mL in DMEM. Final DMSO concentrations in highest test concentration was 0.1%. Stocks were stored in -20 °C. Final dilutions were made in appropriate cell culture medium to the tested concentrations. Supplemental cell treatment started on day 0 of differentiation and continued through day 20 in H9 hESCs and hFF cells. Medium, including chemical dilutions, were made fresh and changed every other day.

2.3.4 Detection of Calcium

Quantification of calcium content was performed using a calcium assay normalized to protein content. Cells were lysed with radio-immunoprecipitation (RIPA) buffer (1% NP40, 0.5% sodium deocycholate, 0.1% sodium dodecyl sulfate, phosphate buffered saline (PBS)) on day 20 of cellular differentiation. Remaining matrix was washed with 1 N HCl and collected. Both lysates were assayed with Arsenazo III (Genzyme), and absorbance was measured at 655 nm (iMark microplate reader; BioRad). Absorbances were compared to a $CaCl_2$ standard and total calcium content was normalized to total protein content determined by a Lowry assay (Davis et al., 2011). The Lowry assay was read at 750 nm (iMark microplate reader; BioRad) after a 15-minute micro-shake incubation and total protein was determined by comparing to a BSA standard curve.

2.3.5 MTT Assay

Viability response to constituent exposure was determined by 3-[4,5-dimethylthiazol-2yl]-2,5-diphenylterazolium bromide (MTT) assay. Cells were incubated with MTT (5 mg/ml) at 37 °C for 2 h. Following incubation, the supernatant was removed and replaced with 0.04 mol/L HCl in isopropanol. The plate was placed on a shaker for 15-minutes to dissolve aggregates. The optical density of the solution was read at 595 nm (iMark microplate reader; BioRad) (zur Nieden et al., 2010; zur Nieden & Baumgartner, 2010; Walker et al., 2014).

2.3.6 Statistical Analysis

Half-maximal inhibitory doses of cytotoxicity (IC_{50}) and osteogenic differentiation (ID_{50}) were taken from concentration-response curves (nonlinear regression; GraphPad Prism)

and embryotoxicity classes calculated according to Genschow et al. (2000; 2002). A biostatistical prediction model based on linear discriminant functions was employed to correctly classify the test chemical into one out of three total embryotoxicity categories (strong, weak, and non-embryotoxic) (Genschow et al., 2002). Within the formulae, calculated ID_{50} concentrations are relatively compared to the chemical IC_{50} counterpart. All exposures were performed in biological quintuplicates.

2.4 Results

2.4.1 *mEST v. hEST Screenings.* To mirror previous EST comparisons, a training set of chemicals (**Table 2.1**) was tested to establish the predictivity of how the human-cell-based assay compares to the current standard. Cells were concomitantly exposed to the selected chemicals during differentiation to osteoblasts to obtain a half-maximal inhibitory concentrations based on the two endpoints of cytotoxicity and matrix calcification. The

	hEST				mEST			
Chemical	H9 ID_{50}	H9 IC_{50}	hFF IC_{50}	Devtox cat	D3.6 ID_{50}	D3.6 IC_{50}	3T3 IC_{50}	Devtox cat
17α-Estradiol	3.65	14.48	12.96	I	>10	16.54	8.445	I
5,5-Diphenyl-hydantoin	63.29	5.497	7.265	I	>10	228.6	1.981	I
Coumarin	17.47	15.18	57.1	III	>10	6.542	0.204	II
Cyclohexamide	0.4203	0.1649	0.293	III	0.9382	0.02923	0.08589	III
17α-Ethinylestradiol	4.47	10.13	10.64	I	>10	12.18	1.82	I
Chlorpyrifos	0.01738	500.9	>10	II	>10	>10	4.848	II
DEET	0.01362	281.2	6.996	II	>10	282.6	1.143	I
Folic acid	5.85	>1,000	5.076	I	>10	>10	194.8	I
1,3-Dibromo-5,5-dimethylhydantoin	0.05601	16.37	0.000646	II	>10	18.03	25.4	I
Acetaminophen	6.364	9.986	15.22	III	>10	6.621	5.725	II
Norgestrel	0.0771	2.915	8.696	II	>10	>10	>100	II
3,3',5,5'-Tetra-bromobisphenol A	9.52	>10						
Benz(a)anthracene	205.8	171.7	>1,000	I				
Cyclopamine	7.546	9.88	40.9	I				
Abamectin		3.799						
Sodium saccharin hydrate	1,000	>1,000		I	>1,000	>1,000		I
Hexaconazole	11.18	>100						
Raloxifene hydrochloride		7.72						
Quinoline	2.269	2.648	59.42					
Tetracycline	0.5539	43.34						
Triadimefon	0.4070	11.2900	29.29					
Disulfiram	3.541	7.72						
Triadimenol	1.0120	9.6960	>100					

Table 2.1 Select screening chemicals and endpoint comparisons. Highlighted boxes depict developmental toxicity category discrepancies between human and mouse EST models.

latter was used to indirectly quantify the amount of mature, functional bone-forming osteoblasts from a calcium assay, normalized to protein content of the cultures. All half-maximal inhibitory concentrations were then related to a half-maximal inhibitory concentration obtained from exposing fully differentiated fibroblasts using three Fisher functions developed for mouse cells. Results from the mEST screening will be used to establish the differential sensitivity of cells from different species and to further converge on the final predictivity of our human-cell-based assay. The initial screenings demonstrate higher concentrations are needed within the mouse model to reach the half-maximal inhibitory threshold (**Supplemental Figure 2.1**).

Next, the above screening chemicals were assessed in hESCs. Initial comparisons were made to determine any notable differences between the *in vitro* model methods. Early test concentrations were performed at lower chemical doses and resulting lower ID_{50}/IC_{50} values were gathered. From the initial screenings, the implementation of this screening technique over current methods is validated as results suggest human exposure has greater sensitivities (**Supplemental Figure 2.2, 2.3**).

Additionally, a regression analysis was performed to directly compare viability to effects on differentiation. This was done by taking the $LogIC_{50}$ and dividing by the $LogID_{50}$. Results can be seen in **Fig 2.2.** This regression analysis demonstrated visual representation on how toxicants are categorized based on embryotoxicity. Highly negative values represent strong embryo-toxicants, values that are close to equal are weak embryo-toxicants, and highly positive values are non-embryotoxic.

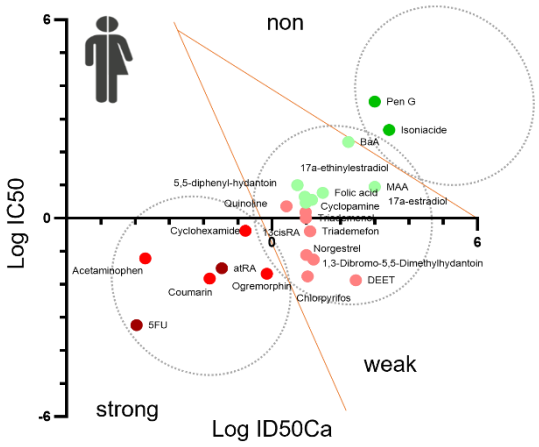

Figure 2.2: LogID_{50} concentrations plotted over LogIC_{50} concentrations to depict relationship between calcium content and cell viability.

2.5 Discussion

The biostatistical model developed for the classic EST has been able to classify the reference control chemicals similarly between species and appropriately matched them to their *in vivo* embryotoxicity. Darker shaded dots indicate a "strong" effect either strongly embryotoxic or non-embryotoxic. Lighter shaded dots fall within the mildly embryo-toxic cateogory. The selected reference control, *13cis*RA was classified as non-embryotoxic (class I) based on the sensitivity of the mouse embryonic stem cells, but as moderately embryotoxic (class II) based on the human ESCs. 13*cis*RA was found to be embryotoxic *in vivo* within humans. The prediction model unscores the neccessity for human relevance within the classic EST. This data demonstrates that some chemicals can have negative outcomes on human osteogenesis, which would not be detected with the current mouse cell-based assay. The sensitivity descrepancies are likely attributed to species-specific differences in exposure, however despite both mESCs and hESCs derived from the ICM of a blastocyst hESCs resemble primed mESCs (Chen and Lai, 2015). Primed mESCs are derived from epiblasts post-implantation (Chen and Lai, 2015).

While most of the chemicals screened demonstrated increased sensitivity to the hESC model, some compounds displayed similar effects between models, where the screening compound's affect on osteogenesis was dependent on cell viabililty. In these cases, cells are dying as a result of exposure and therefore, consequently, cells are not differentiating. For instance, Cyclohexamide exposure elicited nearly identical ID/IC_{50} concentrations. Since Cyclohexamide is a protein synthesis inhibitor that is being applied to a living system this outcome is understandable. The distinct descrepcies of the dependence or independence of cell death is a cruical component in policy making.

However, there were instances in which cell viability was unaffected and osteoblast production was hindered. In particular, the H9 IC_{50} concentration for DEET was 200x greater than the observed ID_{50} concentration. This failure to form osteoblasts but not cause cytotoxicity suggests a differenitation defect due to exposure. DEET is the main component of insect spray and is ubquitiously used in areas with large amounts of water. There is no federal warning issued to pregnant persons to minimize exposure to DEET, therefore results demonstrate the neccessity for more appropriate development-based assays.

Together, these endpoints provide a reliable assessment of the formation of bone-forming osteoblasts, or lack thereof, depending on chemical exposure as method for compound human risk assessment. This hEST osteogenic method, with the inclusion of more test chemicals, will impart a reformed technique to replace animal testing, which is of great use to the EPA.

References

1. Chen, Y., Lai, D. 2015. Pluripotent states of human embryonic stem cells. *Cellular reprogramming.*17(1) DOI: 10.1089/cell.2014.0061

2. Davis, L.A., Dienelt, A., zur Nieden, N.I., 2011. Absorption-based assays for the analysis of osteogenic and chondrogenic yield. Methods Mol. Biol. 690, 255–272.

3. https://www.epa.gov/chemical-research/toxcast-data-generation-toxcast-assays

4. Festag M, Viertel B, Steinberg P, Sehner C. 2007. An *in vitro* embryotoxicity assay based on the disturbance of the differentiation of murine embryonic stem cells into endothelial cells. II. Testing of compounds. *Toxicol In Vitro*. 21(8):1631-40. doi: 10.1016/j.tiv.2007.06.014.

5. Genschow, E., Scholz, G., Brown, N., Piersma, A., Brady, M., Clemann, N., Huuskonen, H., Paillard, F., Bremer, S., Becker, K., Spielmann, H., 2000. Development of prediction models for three in vitro embryotoxicity tests in an ECVAM validation study. *In Vitr. Mol. Toxicol*. 13 (1), 51–66.

6. Genschow E; Spielmann, H; Scholz, G; Seiler, A; Brown, N; Piersma, A; Brady, M; Clemann, N; Huuskonen, H; Paillard, F; Bremer, S; Becker, K. 2002. The ECVAM international validation study on *in vitro* embryotoxicity tests: results of the definitive phase and evaluation of prediction models. Altern. Lab Anim. 30(2):151-76.

7. Orioli IM, Castilla EE, Barbosa-Neto JG. 1986. The birth prevalence rates for the skeletal dysplasias. *J Med Genet.* 23: 328–332.

8. Piersma, A.H. 2004. Validation of alternative methods for developmental toxicity testing. *Toxicol. Lett.* (149)147-153.

9. Richard, A. M., Judson, R. S., Houck, K. A., Grulke, C. M., Volarath, P., Thillainadarajah, I., Yang, C., Rathman, J., Martin, M. T., Wambaugh, J. F., Knudsen, T. B., Kancherla, J., Mansouri, K., Patlewicz, G., Williams, A. J., Little, S. B., Crofton, K. M., & Thomas, R. S. 2016. ToxCast Chemical Landscape: Paving the Road to 21st Century Toxicology. Chemical Research in Toxicology, 29(8), 1225–1251.

10. Spielmann H, Pohl I, Doring B, Liebsch m, Moldenbauer F. 1997. The embryonic stem cell test (EST), an *in vitro* embryotoxicity test using two permanent cell lines: 3T3 fibroblasts and embryonic stem cells. *In Vitro* Toxicology. 10:119–27.

11. Sparks, N. I; Madrid, J. V; Bottom, R; Vera-Colon, M. KM; zur Nieden, N. I. Differential predictivity of human pluripotent stem cell lines in skeletogenic developmental toxicity assays. *CRTOX*. In revision

12. Walker, L., Baumgartner, L., Ast, J., Keller, K.C., Trettner, S., zur Nieden, N.I., 2014. Non-human primate and rodent embryonic stem cells are differentially sensitive to teratogens. *Tox. Reports* 2, 165–174.

13. zur Nieden NI, Kempka G, Ahr HJ. 2003. *In vitro* differentiation of embryonic stem cells into mineralized osteoblasts. *Differentiation.* 71(1):18-27. doi: 10.1046/j.1432-0436.2003.700602.x.

14. zur Nieden, N. I., Kempka, G., & Ahr, H. J. 2004. Molecular multiple endpoint embryonic stem cell test—A possible approach to test for the teratogenic potential of compounds. *Toxicology and Applied Pharmacology*, *194*(3), 257–269.

15. zur Nieden, N.I., Davis, L.A., Rancourt, D.E., 2010. Comparing three novel endpoints for developmental osteotoxicity in the embryonic stem cell test. *Toxicol. Appl. Pharmacol.* 247 (2), 91–97.

16. zur Nieden, N.I., Baumgartner, L., 2010. Assessing developmental osteotoxicity of chlorides in the embryonic stem cell test. *Reprod. Toxicol.* 30(2), 277–283.

CHAPTER 3: FETAL SKELETAL ASSESSMENT OF *IN UTERO* EXPOSURE TO TOBACCO EXTRACTS

3.1 Introduction

Tobacco has numerous utilities and has been a staple in everyday life since 5000 B.C., however the smoking and consumption of tobacco for recreational purposes only began in 1492 (Musk, 2003). Smoking and tobacco use were reported by the US Surgeon General as the most extensively studied source of disease (Musk et al., 2003; US Public Health Service; USDHEW, 1967; USDHEW, 1969), yet regulatory policies and consumption remain unchanged. Diseases implicated or exacerbated by tobacco use are ample, such as heart disease, stroke, multiple organ-specific cancers, premature aging, and infertility (Musk et al., 2003; Winstanley et al., 1995; US Department of Health and Human Services, 1982; US Department of Health and Human Services, 1989; US Department of Health and Human Services, 1990; English et al., 1995). Other tobacco-related risks and diseases include hormonal irregularities, osteoporosis, and other impacts to reproductive health (NIH-b; UCI; Ward et al., 2001). Those often left unmentioned are tobacco-induced birth defects. Women make up a staggering 20% of global smokers (Warner et al., 2005) and 10-12% of those women in the U.S. still consume tobacco products throughout pregnancy (Tong et al., 2009). Stillborn rates associated with *in utero* tobacco exposure were assessed in a cohort of 25,102 singleton pregnancies with a 30% population of pregnant smokers (Wisborg et al., 2001). Findings included a 25% rate of stillbirths and 20% rate of infant deaths (Wisborg et al., 2001).

While tobacco-induced fetal and infant death has a prevalent association and is easily avoidable, birth defects related to *in utero* tobacco exposure is much more difficult to report. There are numerous pregnancy outcomes, aside from mortality, associated with *in utero* tobacco or second-hand exposure, including early delivery, low birth weights, and other newborn measurement assessments (Adgent et al., 2006; Werler et al., 1997). As previously discussed, tobacco use affects heart health, and these implications extend to congenital heart defects in children (Malik et al., 2008). In fact, congenital heart defects make up the most prevalent birth defects and is highly linked to *in utero* tobacco smoke exposure (Cleves et al., 2003; Boneva et al., 2001; Moller et al., 1993; Malik et al., 2008).

In addition to an increased risk for heart defects, tobacco exposure inflicts skeletal birth defects. Many reports indicate 1 in 1000 births have diagnosed defects of the axial skeleton (Cohen et al., 1997; Jaskwhich et al., 2000; Erol et al., 2004; Brent et al., 2007; Dias et al., 2007; Oskouian et al., 2007; Alexander et al., 2010). Of these skeletal defects, 40% coexist with a neural tube defect and 2-5% have additional limb defects (Cohen et al., 1997; Jaskwhich et al., 2000; Erol et al., 2004; Brent et al., 2007; Dias et al., 2007; Oskouian et al., 2007). Exposure to tobacco *in utero* is also known to be associated with malformations of the skeleton, such as a decrease in overall length and head and chest circumferences (Macdonald-Wallis et al., 2011). Extensive epidemiological reports have shown children exposed to tobacco *in utero* have an increased risk of bone malformations, including an increased amount of hypomineralized bones and risk of fracture following minor injuries (CDC). Additional studies reveal that smoking during any point in pregnancy significantly impacts embryonic bone-related measurements, such as overall

total body height, less head bone mineral content, bone age, and bone mineral density (Macdonald-Wallis et al., 2011). Arguably, limited physical mobility wreaks havoc on overall well-being and increases the risk for unwellness in both physical and mental health.

Skeletal birth defects associated with *in utero* tobacco exposure research is neglected as most skeletal defects are seen as simply cosmetic in nature. However, by assessing the development of differentiating hESCs into bone-forming osteoblasts, impacts on embryonic skeletal development can be assessed. Skeletal toxicity has become a popular gauge for assessing toxicants, largely due to the sensitivity of the system and the variety of phenotypes (Toppari et al., 1996). Longitudinal meta-data on potential embryonic tobacco exposure is readily available, however, conditions are limited by participant and results are subjected to outside influences beyond the scope of tobacco exposure.

Despite most of this research surfacing from conventional cigarettes, "harm-reduction" products are becoming increasingly popular to consumers. As an alternative to conventional cigarettes, pregnant smokers will opt to use "harm-reduction" cigarettes because they have lower tar and nicotine content or ultra-filtered, previously advertised as "light" cigarettes. Recently on October 22, 2019, the FDA, for the first time, approved some Snus products—smokeless tobacco pouches that are placed under the lip to allow absorption of nicotine—to be marketed as bearing reduced harm in comparison to combustible cigarettes (https://filtermag.org/fda-snus-harm-reduction). While its product packaging specifies a lower risk of mouth cancer, heart disease, lung cancer, stroke, emphysema, and chronic bronchitis, its negative outcome on skeletal health is unknown.

3.2 Previous Data

To aid in the identification of adverse outcome pathways associated with the recently reported higher bone fracture risks in children exposed to tobacco *in utero* (Parviainen et al., 2017), the lab tested whether the detrimental effect of tobacco products to produce skeletal defects can be recapitulated in the human osteogenesis *in vitro* model (Sparks et al., 2018; see chapter 2). The screen produced two significant new findings: 1) hESCs showed adverse responses to tobacco products: all seven tested products elicited decreases in calcification, thus confirming this model as an excellent *in vitro* tool to unravel molecular mechanisms underlying hypomineralization and bone fracture risk in children (**Fig. 3.1A**). 2) Normalization to nicotine content revealed that extracts from harm-reduction tobacco products, including Snus, were more potent in inhibiting human osteogenesis than extracts from conventional cigarettes, causing osteogenic differentiation inhibition in the absence of cytotoxicity and independent of nicotine (Martinez et al., 2022) (**Fig. 3.1B**). By extension, this data suggests that exposure of a pregnant woman to the harm-reduction products Camel Blue and Snus and the chemicals therein increases the

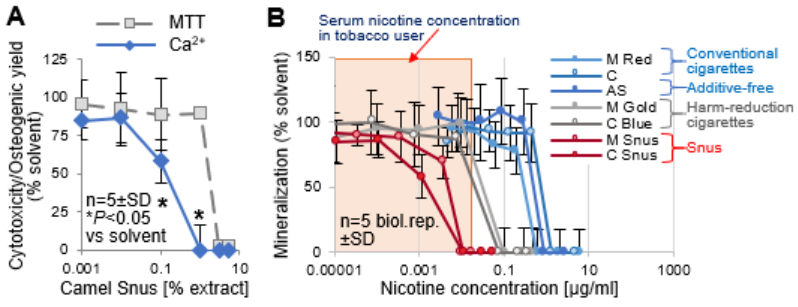

Fig. 3.1 Harm reduction products are inhibitory to human osteogenic differentiation. (A) Concentration response-curves for Snus extract tested on protocol. Effective Dose (ED) = 0.1% Snus tobacco extract. Non-effective Dose (NED) = 0.0005% Snus tobacco extract. Cytotoxicity = MTT assay, Calcification = Ca^{2+} assay. (B) Calcification concentration-response curves for all tested tobacco products normalized to nicotine. Smoke extract was from sidestream smoke. AS, American Spirit; M, Marlboro; C, Camel.

chances of her giving birth to a child with skeletal defects. To validate these findings *in vivo*, in this chapter mouse exposures were conducted, and the skeletons of the offspring analyzed from images.

3.3 Methods

3.3.1 *In Vivo Mating Schedules.* The University of California, Riverside Institution Animal Care and Use Committee have reviewed and approved all mice experimentation outlined below (AUP#A-20180064). A harem pairing of C57/BL6 mice were housed late evening and the next morning each dam was checked for the presence of a vaginal mucous plug. If a plug was present, dams were separated, and timed pregnancy was identified as embryonic (E) stage 0.5. Standard mating ages were used (6-8 weeks old).

3.3.2 In Vivo Tail-vein Injections. On E6.5 and E8.5, tail-vein injections were administered using sterile 28-30 gauge needles with no more than 0.2mL of solution to pregnant dams. Injections contained a saline solution (PBS) (20 dams injected), aqueous Camel Blue extracts (0.13 puff equivalence) (15 dams injected), or aqueous Snus extracts (0.1% w/v) (15 dams injected). Concentrations used for *in vivo* exposure were identified in initial *in vitro* tobacco screenings as the ID_{50} values. These concentrations were normalized against nicotine concentration to determine exposure relevance, and both fall within the concentration of nicotine found within the serum of tobacco users (33 ng/mL).

3.3.3 Embryo Extractions. On E17.5, pregnant dams were weighed and euthanized by a combination of CO_2 gas and cervical dislocation. Following culling, the uterus was dissected and fanned out with pups exposed. Pup litter size was recorded. Pups were then carefully skinned and eviscerated. Organs were removed and flash frozen. Skin, fat, and

muscle were manually removed as effective as possible before placing in a 95% EtOH solution. Remaining tissue was excised with standard dissection scissors. Skeletons were then submerged and fixed in a 4% PFA solution overnight. Following fixation, skeletons were stored in a 1:1 PBS: glycerol solution and then double-stained in Alican Blue and Alizarin Red.

3.3.4 Image J. Measurements were collected for relevant bones via ImageJ. Images were uploaded and scales were set. The segmented line tool was used to precisely obtain the following measurements: femur, ulna, radius, and last single attached rib for total lengths, diameters, and calcified bone lengths not including any mineralization overlap.

3.3.5 Data Processing. Python and R were used and visualized via Jupyter notebook (available upon request) for data processing and statistical analysis, respectively. The analytic approach taken includes a distribution-based comparison, then a more direct statistical comparison. Empirical Cumulative Distribution Function (ECDF) plots were plotted to observe notable changes to distribution between untreated and tobacco-treated groups. P-values for the ECDF plots were calculated based on Kolmogorov-Smirnov (K-S) test statistics. Additionally, measurements were displayed in box-and-whisker plots with a Welch's t-test p-value. $P < 0.05$ was considered significant.

3.4 Results

3.4.1 *Assessment of Femur Bone.* Quality of the femur bone of tobacco extract-exposed pups were assessed using the following quantitative measurements: length of femur, mineralization length of femur, and diameter of femur. Initial unbiased comparisons were performed to determine overall differences to sample distributions using ECDF plots

(**Figure 3.2**). Femur length and diameter were insignificant in Snus embryos, however the calcified bone length distributed was significantly different than the control. Interestingly, Camel Blue embryo distributions were significantly different between femur and calcified bone lengths, but not in diameter.

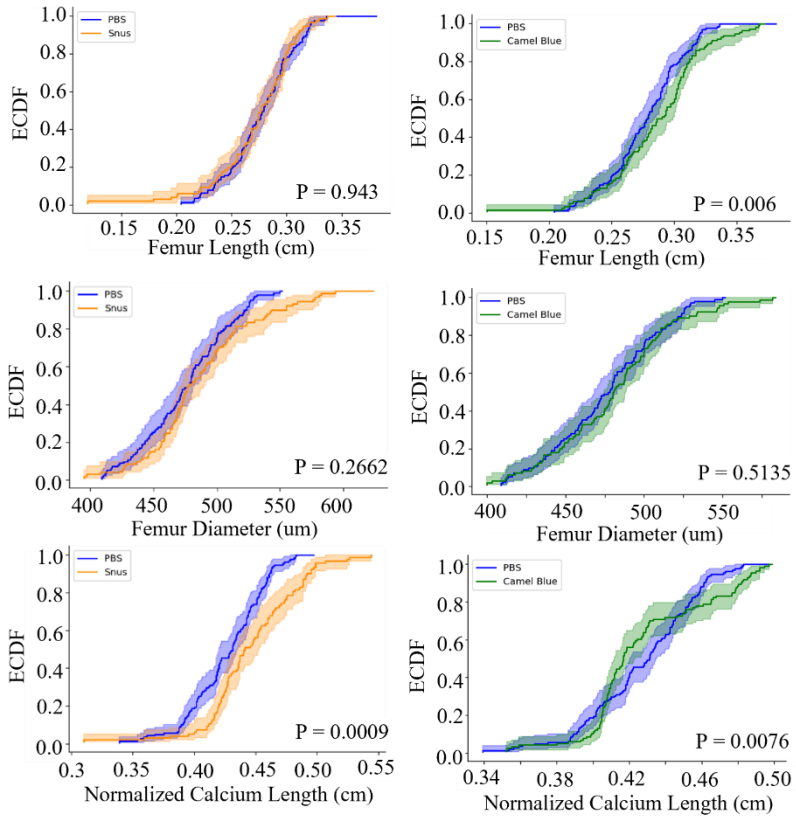

Figure 3.2 Comparison of femur measurements. ECDF were generated to compare distributions and statistical differences of femur measurements collected. ECDF plots of Camel Snus and Camel Blue femur lengths, femur diameters, and calcified femur lengths. Significance indicated by p-value.

There was no effect on femur length (PBS-STE p = 0.1744) (PBS-CB p = 0.1120) in either tobacco-treated sample (**Figure 3.3**). Snus showed significant reduced femur diameter (PBS-STE p = 0.0346), however, there was no difference in the Camel Blue diameters (PBS-CB p = 0.1265). The observable insignificances can likely rule out changes to overall bone health. However, a significant increase in normalized mineralization length

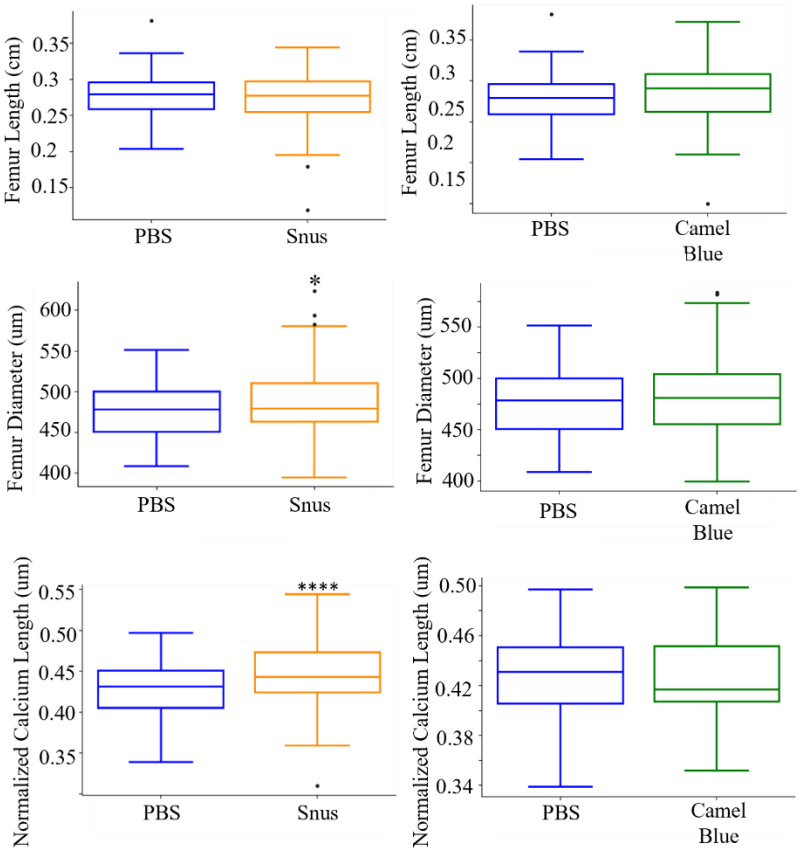

Figure 3.3 Comparison of femur measurements. Box plots were generated to compare distributions and statistical differences of femur measurements collected. Box plots of Camel Snus and Camel Blue femur lengths, femur diameters, and calcified femur lengths. A Welch's t-test was performed. *< 0.05; ****<0.00001. Graphs were plotted via Python and statistics calculated via R.

of Snus-treated pups was seen (PBS-STE p = 1.195e-05) (**Figure 3.3**). No such effect was seen in Camel Blue-exposed pups (PBS-CB p = 0.8478). This may indicate that during duration of embryonic exposure, Snus influenced femur bone integrity and initiated hypermineralization. This is likely attributed to an aberration in regulation of growth factors while development is occurring.

3.4.2 *Assessment of Forearm Bone.* In addition to femurs, forearm parameters were also assessed. The forearm is composed of two major bones, the ulna and radius. Similar to the femur bones, the Snus- and Camel Blue-exposed forearms were assessed using the

following measurements: length of ulna and radius, mineralization length of ulna and radius, and diameter of ulna and radius. Both ulna length and diameter of Snus-exposed embryos were significant (**Figure 3.4**). Both the diameter and ulna length distributions

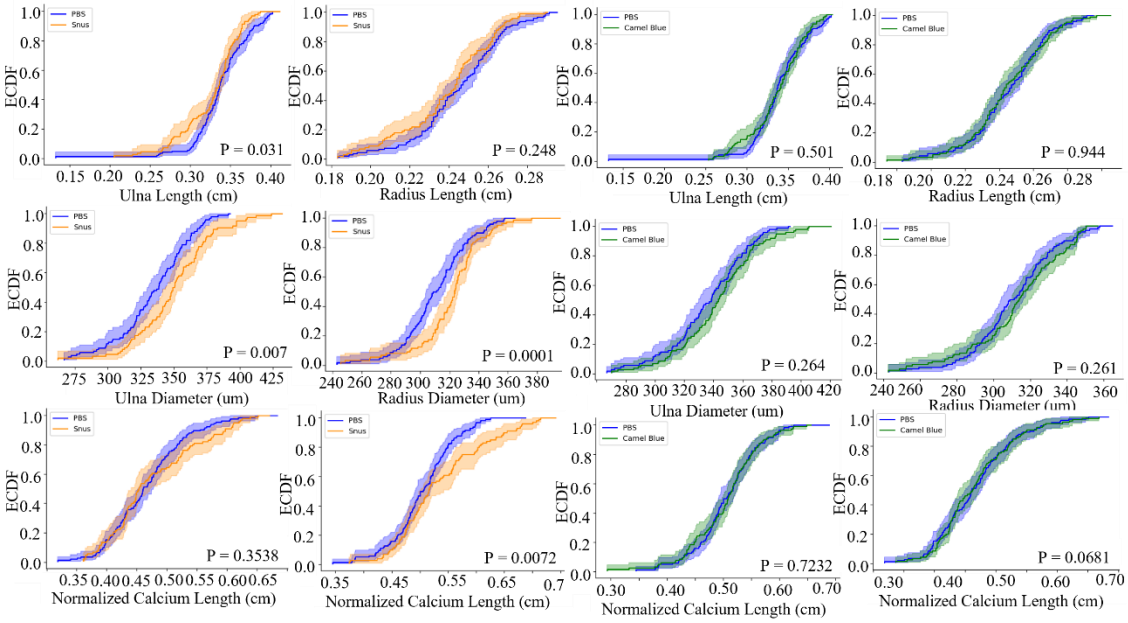

Figure 3.4 Comparison of forearm measurements. ECDF and box plots were generated to compare distributions and statistical differences of the two forearm bones, ulna and radius, measurements collected. ECDF plots of Snus and Camel Blue lengths, diameters, calcified lengths of ulna and radius. Significance indicated by p-value.

were significantly different in Snus embryos; however, the calcified bone length distribution was not. None of the Camel Blue ulna- or radius-related embryo distributions were significant.

Unlike femurs, a significant decrease was seen to the length of the ulnas in Snus-exposed pups (ulna: PBS-STE p = 0.0026), however not Camel Blue treatments (ulna: PBS-CB p = 0.295) and no such effect was seen in the radius (radius: PBS-STE p = 0.2607) (radius: PBS-CB p = 0.4668) (**Figure 3.5**). The ulna diameters of Snus-treated pups were significantly wider than the PBS-exposed controls (ulna: PBS-STE p = 0.0084), but the radius showed no such effect (radius: PBS-STE p = 0.6198). There were no significant

changes in the Camel Blue-exposed forearm diameters (ulna: PBS-CB p = 0.0898) (radius: PBS-CB p = 0.9339). The ulnas in both treatments showed no detected for mineralization length (ulna: PBS-STE p = 0.2895) (ulna: PBS-CB p = 0.8681) (radius: PBS-CB p =

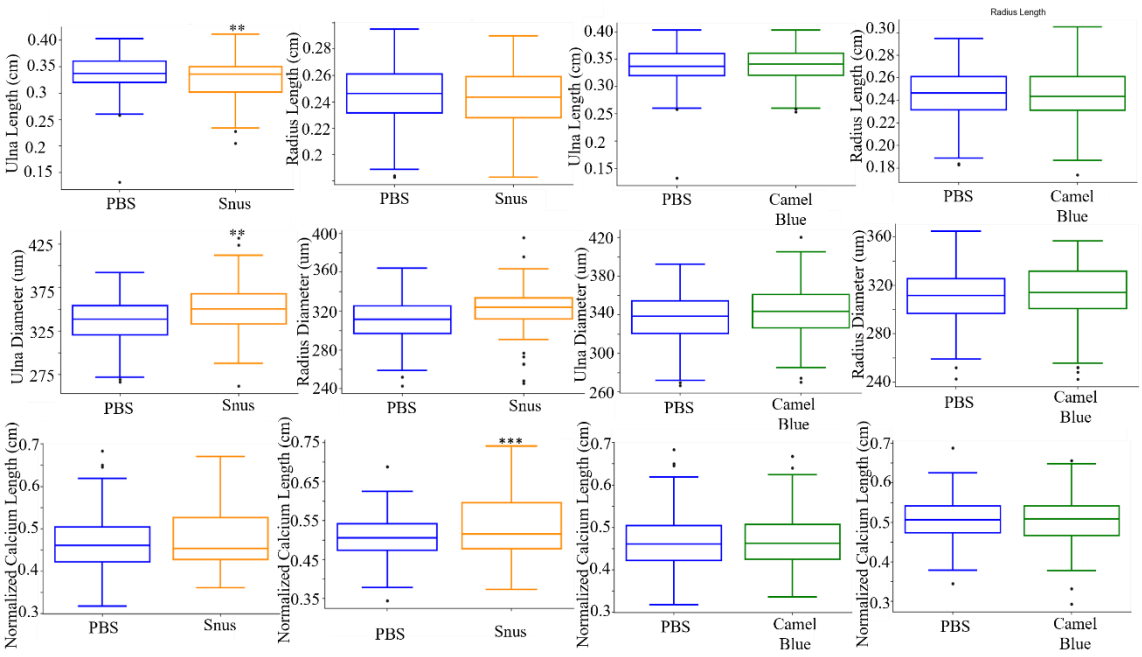

Figure 3.5 Comparison of forearm measurements. Box plots were generated to compare distributions and statistical differences of the two forearm bones, ulna and radius, measurements collected. Box plots of Camel Snus and Camel Blue lengths, diameters, calcified lengths of ulna and radius. A Welch's t-test was performed. **< 0.01; ***<0.0001. Graphs were plotted via Python and statistics calculated via R.

0.8238), but the Snus radii had significantly longer mineralization patterns (radius: PBS-STE p = 0.0008). Embryonic exposure to Snus resulted in major changes to bone health resulting in shorter and wider forearms, while maintaining overall bone integrity.

3.4.3 *Assessment of Rib.* To denote discrepancies between appendicular bones and those that arise via a paraxial mesoderm lineage, a single rib was also assessed. Quality of a single attached rib of tobacco extract-exposed pups were assessed using the following quantitative measurements: length of the last single attached rib and calcified bone length of a single attached rib. Initial unbiased comparisons utilizing ECDF plots to compare

treatment distributions were obtained (**Figure 3.6A**). Rib length was insignificant in Snus embryos; however, the distribution comparison of the calcified rib length was significantly different than the PBS-exposed embryos. A similar trend was seen in Camel Blue, calcified rib length mean distributions were significantly larger, but not the single rib length.

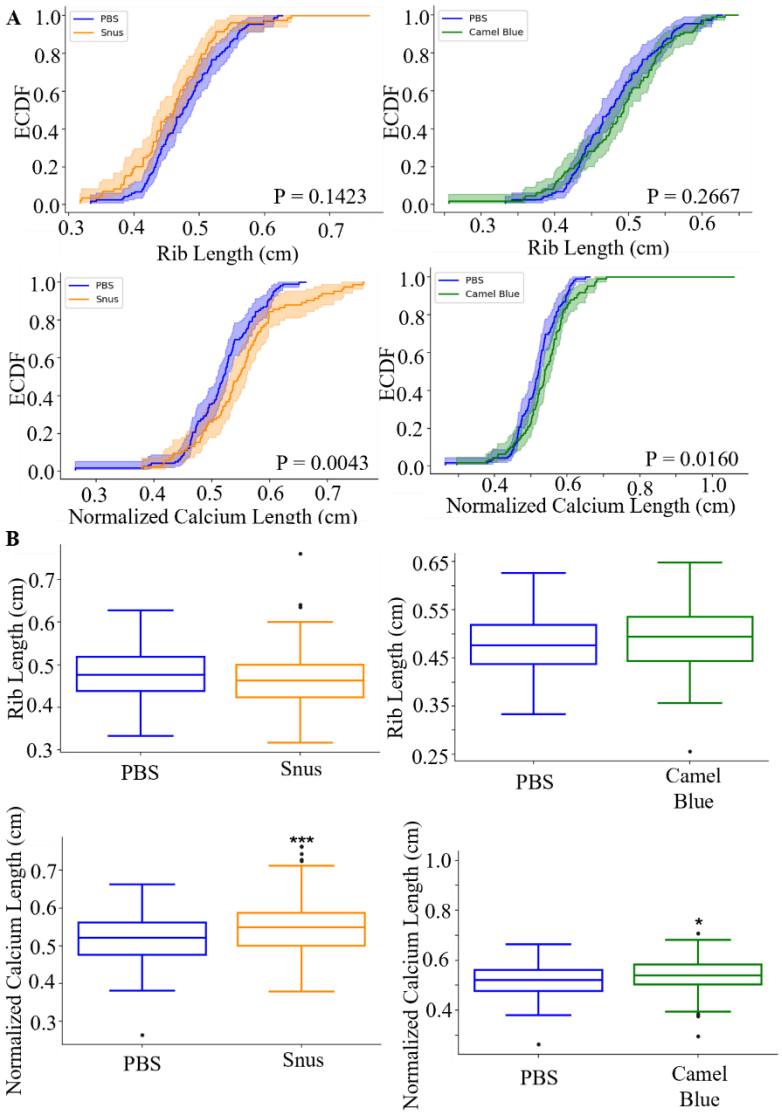

Figure 3.6 Comparison of rib measurements. ECDF and box plots were generated to compare distributions and statistical differences of rib measurements. **(A)** ECDF plots of Snus and Camel Blue single rib lengths and calcified rib lengths. Significance indicated by p-value. **(B)** Box plots of Snus and Camel Blue single rib lengths and calcified rib lengths. A Welch's t-test was performed. *< 0.05; ***<0.0001. Graphs were plotted via Python and statistics calculated via R.

No effect was seen to the rib length (PBS-STE p = 0.06413) (PBS-CB p = 0.2863) in either tobacco-treated samples (**Figure 3.6B**). However, both Camel Blue and Snus had a significantly longer calcified rib length (PBS-STE p = 0.0024) (PBS-CB p = 0.0156). Camel Blue significance in rib bone integrity may indicate bone lineage-specific toxicity.

3.5 Discussion

The distinct pattern of altered calcification *in vitro* can be seen *in vivo* as well. However, *in vivo* models are far more complex especially when considering the convolution of skeletal development. We see a multitude of affected bones due to embryonic tobacco exposure. Additionally, the early, acute exposure model demonstrates the sensitivity of developmental stages when exposure occurs. For instance, hand digit formation coincides with hind limb development. Therefore, despite the appendicular skeleton arising from the same cell types and lineages, specific developmental expression can easily influence one long bone without affecting the other. This is seen even in the slight discrepancies in the ulnae and radii development. The radial bone is naturally smaller in length than the ulna bone (Clemente et al., 2007), however mineralization lengths between the two bones are seen as nearly identical average lengths.

An interesting component to these findings is the consistent changes to bone seen in Snus-exposed embryos. While Camel Blue is considered a “harm-reduction” product, it does contain more constituents than the nine known carcinogens found in smokeless tobacco products (McAdam et al., 2019). Additionally, as this is a combustible product, many by-products are produced during the process, such as additional aromatic hydrocarbons, acroleins, and even carbon dioxide (Sterling et al., 1982). Both tobacco

products contain major carcinogens, such as benz(a)pyrene, yet Snus only displayed changes to bone health. A caveat to this interpretation is that each tobacco product targets a specific bone lineage over another, or Snus products contain lower concentrations of individual constituents. As Snus tobacco extracts were administered via tail-vein injection directly into the bloodstream, the extracts would readily be metabolized across the placental barrier. With Camel Blue, the sidestream smoke exposure approach certainly is a relevant exposure to pregnant women as it includes second-hand exposure; however, the direct bloodstream route neglects metabolites that are formed via route of inhalation. Therefore, the discrepancies seen in bone outcomes between harm-reduction products could be isolated to lack of placental metabolism associated with exposure. Despite both extracts being directly inserted into the bloodstream, it is unclear what metabolites are created during exposure and how that influences development. Final analyses seem to indicate that Snus exposure affects mesoderm-derived bones, such as the forearm and femur, more so than neural crest-derived bones. Additionally, this argument is further validated as significant changes to Camel Blue-exposed embryos only occurred in the ribs. Snus ribs also elicited a significant change to mineralization. Therefore, it appears Camel Blue is more selective to specific bone lineages and the sidestream smoke aspect has a more targeted effect compared to the smokeless tobacco product.

Despite both long bones (forearm and femur) being derived from the same precursor-lineage the overall effects on bone morphology were variable. It appears embryonic Snus exposure resulted in decreased ulna length and a wider diameter in both ulnas and radii which is an indicator of ulna dysplasia. Being that femur development is

slightly delayed in comparison to forearm bones (Bininda-Emonds et. al., 2007), this could explain the changes seen in overall bone morphology in forearm development and not the femur. While the chosen exposure regimen recapitulates early and acute exposure to tobacco during development, our significant findings have implications beyond acute exposure. At glance, these phenotypes are seemingly minor changes to bone formation. However, changes to bone development *in utero* can cause detrimental effects later in life, as commonly seen in epidemiological studies that show an increase of osteoporosis and other related bone diseases, including a greater risk for fractures, in patients born to chronic smoking parents.

References

1. Adgent MA. Environmental tobacco smoke and sudden infant death syndrome: a review. *Birth Defects Research* (Part B). 2006;77:69–85.

2. Alexander, PG; Tuan RS. 2010. Role of environmental factors in axial skeleton dysmorphogenesis. *Birth Defects Research.* 90: 118-132.

3. Bininda-Emonds, O. R., Jeffery, J. E., Sánchez-Villagra, M. R., Hanken, J., Colbert, M., Pieau, C., Selwood, L., ten Cate, C., Raynaud, A., Osabutey, C. K., & Richardson, M. K. 2007. Forelimb-hindlimb developmental timing changes across tetrapod phylogeny. *BMC Evolutionary Biology*, *7*(1), 182.

4. Boneva RS, Botto LD, Moore CA, Yang Q, Correa A, Erickson JD. Mortality associated with congenital heart defects in the United States: trends and racial disparities, 1979 –1997. *Circulation.* 2001;103(19):2376 –2381

5. Brent RL, Fawcett LB. 2007. Developmental toxicology, drugs, and fetalteratogenesis. *Clinical obstetrics: the fetus and mother. Black-well.* pp.217–235.

6. CDC. *Morb. Mortal. Wkly. Rep*. 2008;57: 849–852.

7. Clemente, Carmine D. 2007. Anatomy: A Regional Atlas of the Human Body (5th ed.), Philadelphia, PA: *Lippincott Williams & Wilkins*

8. Cleves MA, Ghaffar S, Zhao W, Mosley BS, Hobbs CA. Firstyear survival of infants born with congenital heart defects inArkansas (1993–1998): a survival analysis using registry data. *Birth Defects Res Part A Clin Mol Teratol.* 2003;67(9):662– 668

9. Cohen MM. 1997. The child with multiple birth defects. *Oxford University Press.*

10. Dias MS. 2007. Normal and abnormaldevelopment of the spine. *NeurosurgClin N Am* 18:415–429.

11. English DR, Holman CDJ, Milne E. 1995. The Quantification of Drug Caused Morbidity and Mortality in Australia. *Commonwealth Department of Human Services and Health.*

12. Erol B, Tracy MR, Dormans JP. 2004. Congenital scoliosis and verte-bral malformations: characterizationof segmental defects for geneticanalysis. *J Pediatr Orthop* 24:674–682.

13. https://filtermag.org/fda-snus-harm-reduction/

14. Jaskwhich D, Ali RM, Patel TC. 2000. Congenital scoliosis. *Curr OpinPediatr* 12:61–66.

15. Macdonald-Wallis, C; Tobias, JH; Smith, GD; Lawlor, DA. 2011. Parental smoking during pregnancy and offspring bone mass at age 10 years: findings from a prospective birth cohort. *Osteoporos Int.* 22:1809–1819. DOI 10.1007/s00198-010-1415-y

16. Malik, S; Cleves, MA; Honein, MA; Romitti, PA; Botto, LD. 2008. Maternal Smoking and Congenital Heart Defects. 121(4) e810-e816. doi:10.1542/peds.2007-1519

17. Martinez IKC, Sparks NRL, Talbot P, zur Nieden NI. Harm-reduction tobacco products cause osteoblast teratogenesis in the absence of cytotoxicity. *Reproductive Toxicology,* under review.

18. Martinez IKC, Sparks NRL, Madrid JV, Talbot P, zur Nieden NI. Exposure to cigarette smoke impedes human osteoblast differentiation independently of nicotine. *Nicotine and Tobacco Research, in press*

19. Martinez IKC, Sparks NRL, Talbot P, zur Nieden NI. Harm-reduction tobacco products cause osteoblast teratogenesis in the absence of cytotoxicity. *Reproductive Toxicology,* under review.

20. McAdam, K.G., Kimpton, H., Faizi, A. 2019. The composition of contemporary American and Swedish smokeless tobacco products. *BMC Chemistry* **13,** 31. https://doi.org/10.1186/s13065-019-0548-0

21. Moller JH, Allen HD, Clark EB. 1993. Report of the task force on children and youth. American Heart Association. *Circulation.* 88(5 pt 1):2479 –2486

22. Musk, A. W; Klerk, N. HDE. 2003. History of tobacco and health. *Respirology.* 8, 286–290.

23. NIH Osteoporosis and Related Bone Diseases National Resource Center. Smoking and Bone Health. 2018. https://www.bones.nih.gov/health-info/bone/osteoporosis/conditions-behaviors/bone-smoking

24. Oskouian RJ Jr, Sansur CA, ShaffreyCI. 2007. Congenital abnormalities ofthe thoracic and lumbar spine. Neu-rosurg Clin N Am 18:479–498.

25. Parviainen R, Auvinen J, Pokka T, Serlo W, Sinikumpu JJ. 2017. Maternal smoking during pregnancy is associated with childhood bone fractures in offspring – A birth-cohort study of 6718 children. *Bone.* 101:202-205.

26. Sterling, T. D., Dimich, H., Kobayashi, D. 1982. Indoor Byproduct Levels of Tobacco Smoke: A Critical Review of the Literature, *Journal of the Air Pollution Control Association*, 32:3, 250-259, DOI: 10.1080/00022470.1982.10465397

27. Tong VT, Jones JR, Dietz PM, D'Angelo D, Bombard JM, CDC. 2009. Trends in smoking before, during, and after pregnancy - Pregnancy Risk Assessment Monitoring System (PRAMS), United States, 31 sites, 2000-2005. *MMWR Surceill Summ.* 58(4):1-29.

28. Toppari J, Larsen JC, Christiansen P, Giwercman A, Grandjean P, Guillette LJ Jr, Jégou B, Jensen TK, Jouannet P, Keiding N, Leffers H, McLachlan JA, Meyer O, Müller J, Rajpert-De Meyts E, Scheike T, Sharpe R, Sumpter J, Skakkebaek NE. 1996. Male reproductive health and environmental xenoestrogens. *Environ Health Perspect.* 104 Suppl 4(Suppl 4):741-803. doi: 10.1289/ehp.96104s4741. PMID: 8880001; PMCID: PMC1469672.

29. UCI Health. What smoking does to your bones. 2018. https://www.ucihealth.org/blog/2018/11/smoking-bone-health

30. US Public Health Service. Smoking and Health. Report of the Advisory Committee to the Surgeon General of the Public Health Service (Washington). US Department of Health Education and Welfare (PHS) 1103. 1464

31. USDHEW. The Health Consequences of Smoking. A Public Health Service Review, 1967: PHS 1696.

32. USDHEW. The Health Consequences of Smoking. A Public Health Service Review, 1969.

33. US Department of Health and Human Services. The Health Consequences of Smoking. Cancer. A report of the US Surgeon General. US Department of Health and Human Services. Public Health Service, Office on Smoking and Health, Rockville, 1982; DHHS (PHS) 82–50179

34. US Department of Health and Human Services. Reducing the Health Consequences of Smoking: 25 Years of Progress. A report of the Surgeon General. US Department of Health and Human Services, Public Health Service, Centers for Disease Control, Center for Chronic Disease Prevention and Health Promotion, Office on Smoking and Health, 1989; DHHS (CDC) 89–8411.

35. US Department of Health and Human Services. The Health Benefits of Smoking Cessation. US Department of Health and Human Services, Public Health Service, Centers for Disease Control, Center for Chronic Disease Prevention and Health Promotion, Office on Smoking and Health, 1990, (CDC) 90–8416.

36. Ward KD, Klesges RC. A meta-analysis of the effects of cigarette smoking on bone mineral density. *Calcif Tissue Int.* 2001;68(5):259-270. doi:10.1007/BF02390832

37. Warner KE. (2005). The role of research in international tobacco control. *Am J Public Health.* 95(6): 976–984.

38. Werler MM. Teratogen update: smoking and reproductive outcomes. *Teratology.* 1997;55:382–8.

39. Winstanley M, Woodward S, Walker N. 1995. Tobacco in Australia. Facts and Issues. Victorian Smoking and Health Program.

40. Wisborg, K; Kesmodel, U; Henriksen,TB; Olsen, SF; Secher, NJ. 2001. Exposure to tobacco smoke in utero and the risk of stillbirth and death in the first year of life. *American Journal of Epidemiology.* 154(4) 322-327.

CHAPTER 4: EFFECTS OF PREVALENT TOBACCO CONSTITUENTS ON OSTEOGENIC DIFFERENTIATION

4.1 Introduction

Current tobacco research reports from the use conventional cigarettes or conventional cigarette second-hand smoke. Yet, alternative products are often more popular and attractive to consumers. These alternative products exist in cigarette form but bear a "light" label. Additionally, this includes a variety of smokeless tobacco products that have been revamped since they were first introduced on the market. Previous work has indicated that although light labels and smokeless tobacco products may be perceived as a safer choice, embryonic skeletal development was far more disrupted in these "harm-reduction" products. Based on preconceived notions that these alternatives to conventional cigarettes are safer, pregnant smokers often gravitate towards those advertised as having lower tar and nicotine content, such as "harm-reduction" products. Recently on October 22, 2019, the FDA, for the first time, approved some Snus products—smokeless tobacco pouches that are placed under the lip to allow absorption of nicotine—to be marketed as bearing reduced harm in comparison to combustible cigarettes (filter mag, 2019). While its product packaging specifies a lower risk of mouth cancer, heart disease, lung cancer, stroke, emphysema, and chronic bronchitis, its negative outcome on skeletal health is unknown. Although smokeless tobacco contains less constituents and lower concentrations of chemicals compared to conventional tobacco products, Snus does contain notable amounts of nicotine, tobacco-specific nitrosamines (TSNAs) and polycyclic aromatic hydrocarbons (PAHs), aldehydes, and cadmium (Environ, 2013). These constituents are all

listed under the FDA's published list containing 93 Harmful or Potentially Harmful Constituents (HPHCs) that are likely the key culprits in tobacco-related diseases (US FDA, 2012). Current regulatory policies are weak and do a poor job of reducing the use of tobacco products. Arguably, with increasing attractiveness of products, there are more consumers than ever before. As previously highlighted, tobacco research and tobacco-induced health effects are well-discussed in the literature, yet consumers continue to utilize these products. Despite the decade's worth of research, the issue to be addressed falls on policy makers, more specifically with more restrictive guidelines and the publication of ingredient lists accessible to the public.

Several studies have found a reproducible, consistent phenotype of hypomineralization in multiple bones of both mice and zebrafish when exposed to tobacco smoke extracts during development (Walker et al., unpublished results; Karmach et al., unpublished results). Additionally, epidemiological studies found an increased rate of hypomineralization and risk of fracture following minor injuries (Barry et al., 2008). This phenotype of reduced calcification can also be detected in prior work when differentiating hESCs toward bone-forming osteoblasts are exposed to products during differentiation (Martinez et al., 2018), thereby providing an adequate human *in vitro* model to study tobacco-exposure-mediated hypomineralization. Furthermore, it was hypothesized that an individual constituent or a particular combination of constituents could explain the consistent phenotype seen in epidemiological studies and both *in vivo* and *in vitro* exposures to tobacco during development. Nevertheless, tobacco smoke is composed of thousands of chemicals. However, as previously mentioned the FDA has identified and prioritized 93

chemicals that are labeled as HPHCs found within tobacco smoke (FDA, 2012). Here, we attempt to informatically prioritize and to isolate single constituents or combinations that exacerbate symptoms utilizing a human embryonic stem cell (hESC) osteogenic differentiation model (Sparks et al., 2018; zur Nieden et al., 2003; Trettner et al., 2014; Dienelt et al., 2010).

4.2 Previous Data

While the advantage of using hESCs to gauge skeletal toxicity associated with chemical exposure over other *in vitro* alternatives is apparent in the relevance to human-specific exposure, the relatively long culture duration qualifies as a medium-throughput model. Therefore, testing all chemical constituents found in tobacco, even if they were identified, would be a lengthy and costly undertaking. The identification of potentially harmful tobacco constituents in the HPHC list has substantially reduced the number of chemicals to test down to 93, yet, testing these chemical constituents individually or in assortments would still be a time-consuming and expensive venture. Therefore, to prioritize chemicals for toxicity testing, we applied the Toxicology Priority Index (ToxPI) Graphical User Interface developed by the Environmental Protection Agency (EPA) in conjunction with the University of South Carolina at Chapel Hill (Reif, 2010) using data from Tox21 and Toxcast (https://www.epa.gov/chemical-research/exploring-toxcast-data-downloadable-data).

Of the 93 chemicals on the FDA's HPHC list only 46 were found in the toxicity forecaster database; however only 17 of those had complete data sets. For each of these chemicals, 72 assays were exported from the toxicity forecaster dashboard across the five

biological processes. **Fig. 4.1B** shows their ranking according to most likely to be harmful on the left (multiple large pie pieces) to least likely to be harmful on the right (no pie pieces). Benz(a)anthracene (3.717) through N-Nitrosodimethylamine (0.102) had

A

Biological Process	Data Type	Weight	# assays
Cell Proliferation	Assay	1	30
Cell Death	Assay	1	27
Oxidative Phosphorylation	Assay	1	8
Mitochondrial Depolarization	Assay	1	5
Cell Morphology	Assay	1	2

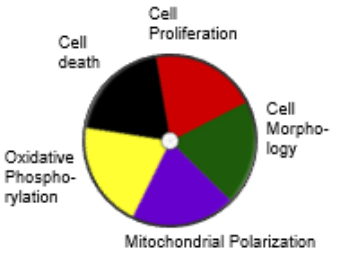

B

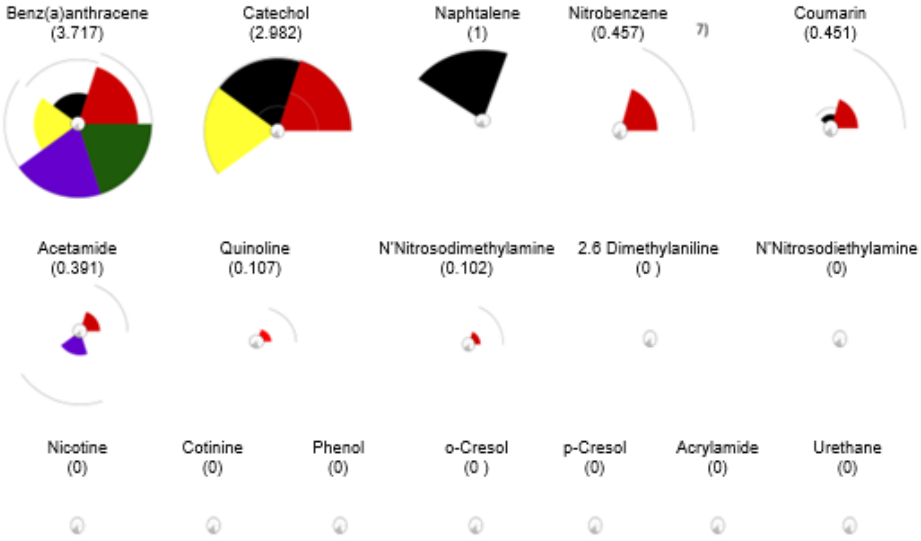

C

	Benz(a)anthracene	Coumarin	Catechol	Quinoline
AC_{50} hit µM Average	47.04	62.51	14.70	67.80
AC_{50} hit µg/mL Average	10.73	9.86	1.16	8.76
H9 hESC ID_{50}/IC_{50} µg/mL	200 ± 76	20 ± 10	0.01 ± .005	2 ± 1.5

Figure 4.1 ToxPI Generated Charts. (A) Table listing the parameters loaded into ToxPI. Each of the five selected biological process was given its own pie chart slice based off assay data and had equal weight. In total, 72 assays encompassed all five biological process slices. Each slice was given its own color. **(B)** ToxPI charts were generated for 17 chemicals using 72 *in vitro* assays across 5 biological processes. **(C)** Toxicity Forecast data averages and *in vitro* H9 hESC ID_{50}/IC_{50} µg/mL values. The average assay hit value in µM (AC_{50}) values for each of tested ToxPI positive constituent obtained from the Toxicity Forecaster database. The AC_{50} in µM for was then converted into µg/mL in comparison to the H9 hESC ID_{50}/IC_{50} values calculated from the *in vitro* osteogenic screen.

designated “hits” and produced positive ToxPI values (0< X). The remainder of the chemicals were identified with null effects (0=X) (**Fig. 4.1B**).

Dose-response Curves Revealed Skeletal Toxicity for ToxPI Positive Chemicals

To then test these chemicals for their embryotoxic potential and validate the predictions, hESCs were induced to undergo osteogenesis from overgrowing cultures with addition of vitamin D_3 (Sparks et al., 2018). This differentiation protocol, while primarily generating osteoblasts from the neural crest, will still form osteoblasts derived from the mesoderm and will therefore identify chemicals with the potential to disturb any type of skeletal formation. Of the seven ToxPI positive chemicals, catechol, coumarin, and quinoline were selected for further analysis as these constituents were identified as embryo-toxic. The MTT and calcium assay, corresponding to cell viability and osteogenic differentiation, respectively, revealed three of the four ToxPI positive predictions (0<X) exhibited severe dose-dependent responses in cytotoxicity and differentiation inhibition (**Fig. 4.2A**).

Catechol exposure caused a decrease in calcification and viability that went in line with the ToxPI predictions. Catechol produced a change in cell viability toward the hFF cell line above 0.882 µg/ml (**Fig. 4.2A**,**B**). Around this concentration range half-maximal inhibitory doses had been reached for cytotoxicity and differentiation inhibition with the hESC cell line. As in the case of benz(a)anthracence, the dose response curves for cell viability and calcification closely followed each other, and hence any developmental

osteotoxicity may be caused by the general cytotoxicity of the compound. The biostatistical model predicted catechol as strongly embryotoxic.

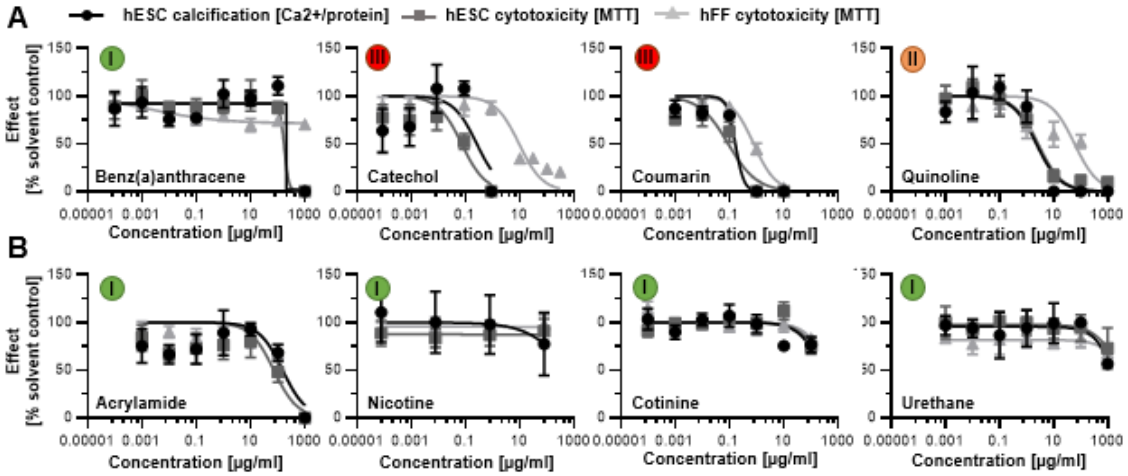

C

Chemical	IC_{50} MTT HFF	IC_{50} MTT hESC	ID_{50} Ca2+ hESC	Embryotoxicity class
Benz[a]anthracene	1000.00	171.70±2.45	205.80±7.88	I
Catechol	9.29±1.71	0.071±0.023	0.258±0.166	III
Coumarin	0.78±0.083	0.0898±0.029	0.164±0.093	III
Quinoline	59.42±19.1	2.65±0.51	2.27±0.76	II
Acrylamide	148.70±33.99	71.02±26.07	150.00±63.1	I
Nicotine	>1000	>1000	633.2±2354	I
Cotinine	496.7±138.9	340.6±72.89	271.6±82.84	I
Urethane	>1000	>1000	>1000	I
Acetaldehyde	0.5647±0.008	0.1522±0.197	0.1710	III
Acrolein	0.0466±0.007	1.809±0.51	1.207±0.33	III
Benzo[a]pyrene	1023±653	52.92±428	2.11±0.65	II
Benzo(b)fluoranthene	110.4±76.08	61.05±14.75	25.78±7.237	I
Isonicotine	>100	>100	>100	I

Figure 4.2. Dose-response Curves for ToxPI-prioritized chemicals. Calcification inhibition and cytotoxicity were measured in hESCs exposed to the indicated chemicals for 20 days. Concentration-response-curves were generated with GraphPad Prism. **(A)** ToxPI positive chemicals. **(B)** ToxPI negative chemicals. **(C)** Respective IC_{50} and ID_{50} values and calculated embryotoxicity classes.

For coumarin, the ToxPI program predicted a marginal toxicity and thus, expectations for the experimental validation of its toxicity were uncertain. hFF and H9 cell viability, and H9 differentiation potential was reduced in the same concentration range, with the hFFs being slightly less sensitive to the compound. With the dose response curves of H9 cell viability and calcification again following similar trends, it is believed that the decrease in calcification might be an attributed consequence of the overall reduction in viable cells. Thus, a 0.152 µg/mL IC_{50} was determined for the H9 hESC line. hFF viability

was also reduced as concentration of coumarin increased. Linear interpolation determined an IC_{50} of 0.0571 µg/mL for hFF cells. To ultimately judge the danger associated with coumarin exposure to the developing skeleton, again, the biostatistical model was applied. As in the case of catechol, it generated an embryotoxicity class of III, strong embryotoxic. Quinoline also elicited greater sensitivity in the hESC endpoints than in the hFF cells and again the curve for the differentiation inhibition closely followed the cytotoxicity curve. Yet, the half-maximal inhibitory concentrations ranged about a decade higher than for coumarin and catechol. Interestingly, the predictive value of each ToxPI assay hit rate in µg/mL was relatively close to the half-maximal inhibitory concentrations experimentally observed *in vitro* for the H9 hESCs for all four tested chemicals (**Fig. 4.1C**).

While H9 hESCs showed a decrease in calcification and cytotoxicity in response to benz(a)anthracene as with the other three chemicals, the decrease occurred at a relatively high concentration - both the half-maximal inhibitory dose for cytotoxicity (IC_{50}) and the half-maximal differentiation inhibitory dose (ID_{50}) were determined at 500 µg/ml, just shy of 1000 µg/ml, which is the highest dose tested in this assay (Genschow et al., 2000; Genschow et al., 2002; Scholz et al., 1999). With the dose response curves of H9 cell viability and calcification following similar trends, it is also likely that the decrease in calcification is an attributed consequence of the overall reduction in viable cells. Against ToxPI predictions, benz(a)anthracene exposure did not produce a change in cell viability toward the hFF cell line for the tested concentration range up to 1000 µg/mL (**Fig. 4.2**). It is often the non-embryotoxic chemicals that produce half-maximal inhibitory concentrations in such high concentration ranges, and indeed a biostatistical model

classified benz(a)anthracene as non-embryotoxic (zur Nieden et al, 2004; Walker et al., 2014; Walker et al., 2021). Other factors that may have influenced exposure discrepancies in cell lines, such as chemical partitioning can be considered minute as all cell lines were plated using the same plastic plating at the same circumference ($0.95cm^2$) and a DMSO control was also utilized to account for the solvent.

Human In Vitro Data for ToxPI Negative Chemicals

Four ToxPI null chemicals (nicotine, cotinine, urethane, and acrylamide) were also taken through *in vitro* screening. ToxPI predicted null effects matched *in vitro* screen data as urethane, cotinine, and nicotine exposure did not inhibit cell viability for either the H9 and hFF cell lines for all tested concentration ranges (**Figure 4.2B**). Likewise, H9 hESC differentiation potential was not altered in the same concentration range for urethane and cotinine. However, a decrease in calcification was seen in the higher concentrations of nicotine exposure. Acrylamide, in turn, caused reductions in cell viability as well as calcification, but in very high concentration ranges. Of these four chemicals tested, all were predicted to have non-embryotoxic effects when employing the biostatistical model (**Figure 4.2C**), in line with the ToxPI predictions.

Screening of Additional Tobacco Constituents

In addition to the 17 chemicals, we identified from the HPHC list using ToxPI, we also selected five more based on existing developmental toxicity data: acetaldehyde, benzo[a]pyrene, acrolein, bezo(b)fluoranthene and isonicotine (Lasker and Younus, 2019; Klingbeil et al., 2014; Moghe et al., 2015; Ratajczak et al., 2021). These constituents are found consistently in tobacco products and smoke, which is highly correlated with

instances of osteoporosis in adults. The first three were existent in the database, however with incomplete assays. Using AC_{50} concentrations from the available proliferation assays generated positive ToxPI charts. When screened with the human *in vitro* model of skeletogenesis, acetaldehyde, benzo[a]pyrene, and acrolein caused differentiation inhibition and cytotoxicity as predicted (**Figure 4.3**), while benzo(b)fluoranthene and isonicotine did not. Notably, differentiation was inhibited at slightly lower concentrations as viability in the case of benzo[a]pyrene exposure, potentially pointing to a differentiation defect that is decoupled from cell death.

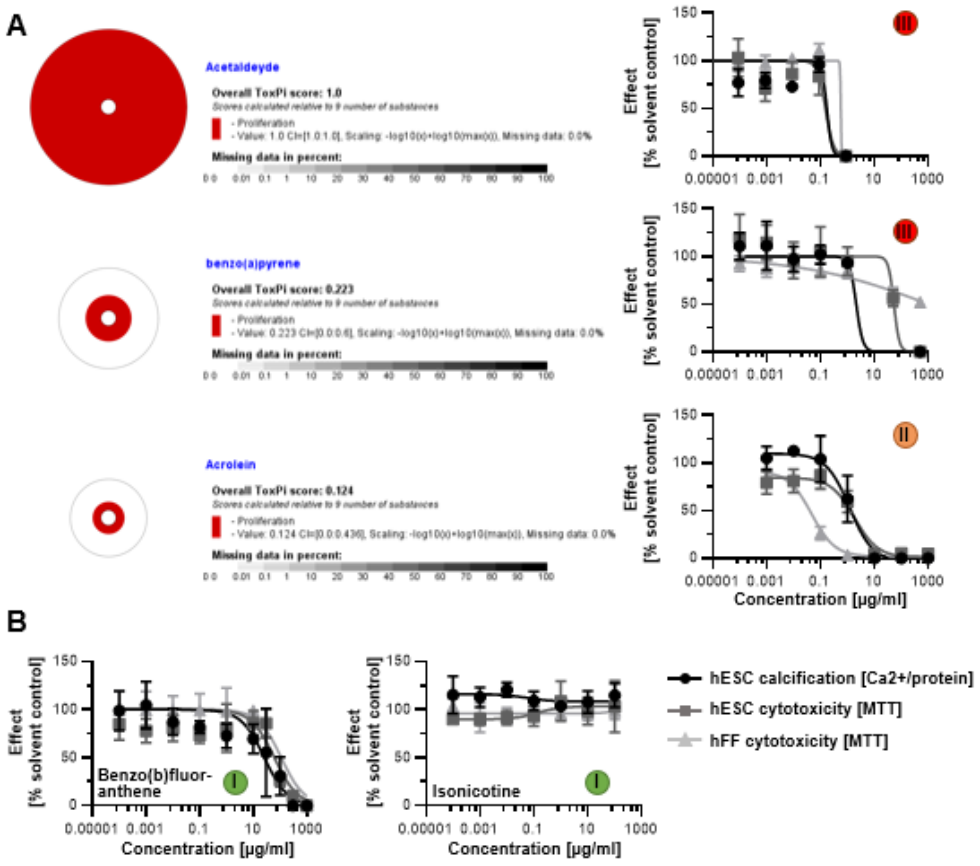

Figure 4.3 ToxPI charts and concentration-response-curves for additional constituents in tobacco.

In addition to the identified ToxPI positive and null chemicals**,** constituents that are present in third-hand smoke (THS) were also screened. These constituents include the tobacco-specific nitrosamines NFN, NAT, and NNK (Acuff et al., 2016). THS is the residue that remains on surfaces after a cigarette has been smoked (Acuff et al., 2016). The presence of THS can remain undisturbed on household surfaces for many months. Despite the HPHC list encompassing mostly mainstream and sidestream components, these three tobacco-specific nitrosamines were included. Despite its presence in the HPHC list, the THS constituents were not identified within the ToxPI analysis, due to the insufficient assays available within the database. However, the screened THS constituents, NFN, NAT and NNK did not elicit cytotoxic or differentiation effects in neither the hFF nor the H9 cell lines (**Figure 4.4**).

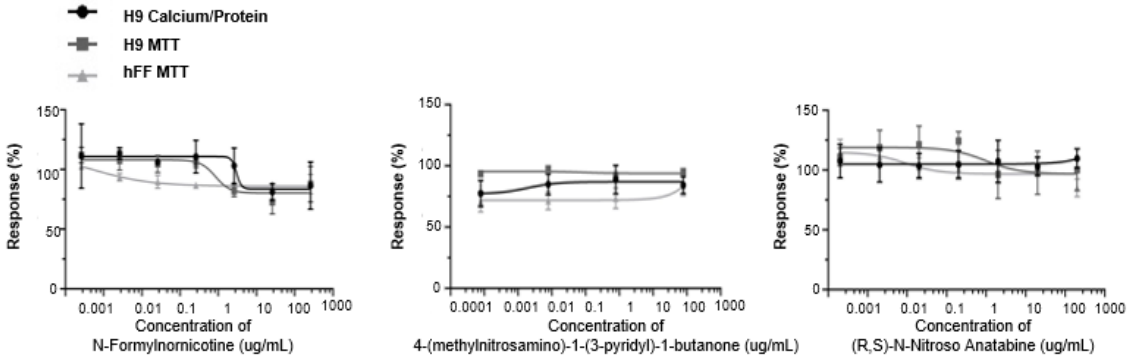

Figure 4.4 THS constituents Dose-response Curves. All three THS constituents did not exhibit toxicity. Curves were graphed via GraphPad Prism. **(A)** N-Formylnornicotine: ID_{50} > 500 µg/mL; IC_{50} (H9) > 500 µg/mL; IC_{50} (hFF) > 500 µg/mL **(B)** 4-(methylnitrosamino)-1-(3-pyridyl)-1-butanone: ID_{50} > 100 µg/mL; IC_{50} (H9) > 100 µg/mL; IC_{50} (hFF) > 100 µg/mL. **(C)** (R,S)-N-Nitroso Anatabine: ID_{50} > 500 µg/mL; IC_{50} (H9) > 500 µg/mL; IC_{50} (hFF) > 500 µg/mL.

4.3 Methods

4.3.1 Cell Culture

H9 human embryonic stem cells (hESCs) were cultured on Matrigel (BD Biosciences) treated culture plates in mTeSR 1 medium (Stem Cell Technologies) at 37 °C with 5% CO_2. Colonies were passaged every 3 days using accutase (2–4 min at room temperature) and a cell scraper to displace colonies from the plastic well. Human foreskin fibroblasts (hFF) cells were maintained in hFF media (DMEM, 10% maintenance FBS, 1% (v/v) non-essential amino acids, 50 U/mL penicillin and 50 µg/mL streptomycin) and plated into a 0.1% gelatin-coated plate. Cells were passaged every 3 days using 0.25% Trypsin-EDTA (5 min at 37ºC).

4.3.2 Osteogenic Differentiation of Human Embryonic Stem Cells

The differentiation protocol established and used within the zur Nieden lab uses confluent H9 hESCs to induce differentiation through the addition of a control differentiation medium (CDM) composed of DMEM, 15% FBS (Atlanta Biologicals), 1% (v/v) non-essential amino acids, 50 U/mL penicillin, 50 µg/mL streptomycin, and 0.1 mM β-mercaptoethanol. CDM is used for the first five days of differentiation to decrease pluripotency. On day five, CDM was supplemented with $1.2*10^{-7}$ M 1,25α$(OH)_2$ Vitamin D_3 (VD_3; Calbiochem), 0.1 mM β-glycerophosphate, and 20.8 µg/mL ascorbic acid.

4.3.3 Exposure to Test Chemicals

Acetaldehyde (Sigma Aldrich, cat. no**.** 402788, 99.5%), Acrolein (Sigma Aldrich, cat. no. 190543, 98%), Acrylamide (Sigma Aldrich, cat. no. 23701, ≤100%), Benz[a]anthracene (Santa Cruz, cat. no. sc-252409, >98%), Benzo[a]pyrene (Toronto

Research, cat. no. B205800, ≤100%), Benzo[b]fluoranthene (Toronto Research, cat. no. B209865, ≤100%), Catechol (Santa Cruz, cat. no. sc-215763, >98%), Cotinine (Sigma Aldrich, cat. no. C5923, 98%), Coumarin (Santa Cruz, cat. no. sc-205637, 98%), Isonicotine (Sigma Aldrich, cat. no. I17508, 99%), Myosmine (Sigma Aldrich, cat. no. M8765, 98%), N-Nitrosoanabasine (NAB) (Sigma Aldrich, cat. no. 75283, 99%), (R,S)-N-nitroso anatabine (NAT) (Toronto Research, cat. no. N524750, ≤100%) N-Formylnornicotine (NFM) (Toronto Research, cat. no. F700875, ≤100%), Nicotelline (Toronto Research, cat. no. N401200, ≤100%), Nicotine (Toronto Research, cat. no. sc-N0267, ≤100%), 4-(methylnitrosamino)-4-(3-pyridyl) butanal (NNA) (Toronto Research, cat. no. M325650, ≤100%), 4-(methylnitrosamino)-1-(3-pyridyl)-1-butanone (NNK) (Toronto Research Chemicals, cat. no. M325750, ≤100%), N′-nitrosonornicotine (NNN) (Sigma Aldrich, cat. no. N075, 90-100%), Quinoline (Sigma Aldrich, cat. no. 241571, 98%), and Urethane (Sigma Aldrich, cat. no. U2500, 99%) components were all identified and prioritized with previously conducted ToxPI analysis. All chemical stocks were diluted to 1,000 µg/mL using DMSO. Further dilutions were made in DMEM (typically 100 µg/mL), depending on identified ID_{50} concentrations. Final DMSO concentrations in highest test concentration was 0.1%. Stocks were stored in -20 °C. Final dilutions were made in appropriate cell culture medium to the calculated ID_{50} concentration. Supplemental cell treatment started on day 0 of differentiation and continued through day 20 in H9 hESCs and hFF cells. Medium, including chemical dilutions, were made fresh and changed every other day.

4.3.4 Detection of Calcium

Quantification of calcium content was performed using a calcium assay normalized to protein content. Cells were lysed with radio-immunoprecipitation (RIPA) buffer (1% NP40, 0.5% sodium deocycholate, 0.1% sodium dodecyl sulfate, PBS) on day 20 of cellular differentiation. Remaining matrix was washed with 1 N HCl and collected. Both lysates were assayed with Arsenazo III (Genzyme), and absorbance was measured at 655 nm (iMark microplate reader; BioRad). Absorbances were compared to a $CaCl_2$ standard and total calcium content was normalized to total protein content determined by a Lowry assay (Davis et al., 2011). Lowry assay was read at 750 nm (iMark microplate reader; BioRad) after a 15-minute micro-shake incubation and total protein was determined by comparing to a BSA standard curve.

4.3.5 MTT Assay

Viability response to constituent exposure was determined by 3-[4,5-dimethylthiazol-2yl]-2,5-diphenylterazolium bromide (MTT) assay. Cells were incubated with MTT (5 mg/ml) at 37 °C for 2 h. Following incubation, the supernatant was removed and replaced with 0.04 mol/L HCl in isopropanol. The plate was placed on a shaker for 15-minutes to dissolve aggregates. The optical density of the solution was read at 595 nm (iMark microplate reader; BioRad) (zur Nieden et al., 2010; zur Nieden & Baumgartner, 2010; Walker et al., 2014).

4.3.6 Statistical Analysis

Half-maximal inhibitory doses of cytotoxicity (IC_{50}) and osteogenic differentiation (ID_{50}) were taken from concentration-response curves (nonlinear regression; GraphPad

Prism) and embryotoxicity classes calculated according to (Genschow et al., 2002; Genschow et al., 2000). A biostatistical prediction model based on linear discriminant functions were employed to correctly classify the test chemical into one out of three total embryotoxicity categories (strong, weak, and non-embryotoxic) (Genschow et al., 2002). Calculated ID_{50} concentrations are relatively compared to the chemical IC_{50} counterpart. All exposures were performed in biological quintuplicates. In double combination analyses, a t-test was performed comparing combination to single constituent ID_{50}. For triple combination analyses, a with one-way ANOVAs with Dunnett's multiple comparison test (single constituent v. combination) using GraphPad Prism. For total combination analyses, a t-test was performed to compare total combination response to an untreated differentiation. A p-value below 0.05 was considered significant.

4.4 Results

4.4.1 *Double Combinatorial Exposures.* It remains to be seen, whether it really is only a single chemical constituent in tobacco smoke that causes the calcification defects or whether it is a mixture of harmful chemicals, whereby some exert positive and others negative effects. To begin answering this question, we next tested combinations of chemicals starting with the chemicals identified as carrying a skeletal embryotoxicity risk from **Fig. 4.2B**. Nicotine was also included due to its prevalence in tobacco products and its highly addictive properties, despite its classification as a ToxPI null chemical.

Dosed at obtained ID_{50} concentrations, 45 different double combinations were tested. As predicted, cytotoxic and effects to differentiation were seen when combining

two chemicals. However, most notable observations depict an overall maintenance of cell survival amongst many of the combinations (**Figure 4.5 left**).

However, combinations containing the chemical Coumarin showed a decrease in cell viability, which led to absence of calcium matrix present in the differentiating cell line. Curiously enough, in otherwise considered harmful combinations, with chemical pairs that are known to be toxic, still maintained cell survival. For instance, despite the individual constituents Quinoline and Catechol both identified as ToxPI positive components and eliciting a low ID_{50} (indicating high toxicity), the combinatorial pair had no effect on cell survival (**Figure 4.5**), however there was a notable decrease in osteogenic differentiation. In fact, Catechol was identified as a positive ToxPI constituent and in most pairs with Catechol, differentiation was significantly reduced, yet there was no effect to viability. This demonstrates the ToxPI analysis was correct in predicting Catechol as an embryo-toxicant. Interestingly, Nicotine, an identified ToxPI null chemical in pair with ToxPI positive chemicals, Coumarin, Catechol, resulted in a significant decrease in both viability and

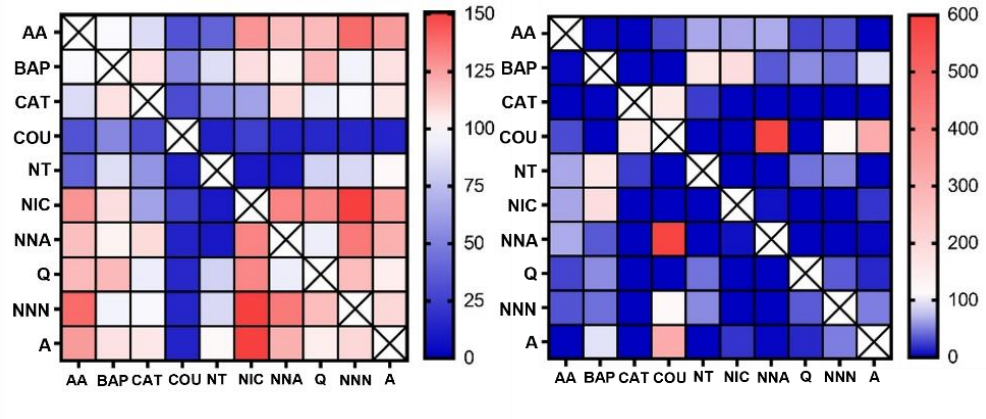

Figure 4.5 Double Combination Heatmaps. MTT (left) and Calcium (right) assays corresponding to double combinatorial exposures. Heatmaps were generated via GraphPad Prism. Data was normalized to Solvent Control (0.1% DMSO). AA = Acetaldehyde / BAP = Benzo(a)pyrene / CAT = Catechol / COU = Coumarin / NT = Nicotelline / NIC = Nicotine / NNA = 4-(methylnitrosamino)-1-(3-pyridyl)-1-butanone / Q = Quinoline / NNN = N-Nitrosonornicotine / A = Acrolein.

differentiation. This likely means these constituents in combination with any non-toxic chemical may still elicit toxicity. Nicotine in combination with Quinoline had no effect on viability but did significantly decrease calcification. Lastly, Benz(a)pyrene, a well-known carcinogen, only significantly reduced differentiation in combination with three chemicals (Acetaldehyde, Catechol, and Coumarin) and in only one instance (Coumarin) of cell viability. It appears this constituent may have some antagonistic properties. Overall, the double combination exposure was able to highlight key combinations (and select chemicals) that demonstrated worsened effects to embryotoxicity. However, it is unlikely that other constituents in the mixture does not change the overall effects of embryotoxicity.

4.4.2 *Triple Combinatorial Exposures.* Similarly, additional combinations were explored using ternary combinations. Dosed at individual ID_{50} concentrations, 10 different sets of triple combinations were tested. Interestingly, the addition of a third chemical did not alter viability or differentiation in respect to most of the double combination exposures. Instead, in some cases the addition of the third chemical appeared to "rescue" the loss of calcification compared to its respective double combination (**Figure 4.6 right**). For instance, the double combination of Quinoline and NNA elicited a significant decrease in calcification, however with the addition of the third constituent, Acrolein, calcification was significantly increased compared to the untreated control. This demonstrates that the addition of any chemical changes the overall effect on survival and differentiation. Above, we highlighted Catechol as affecting differentiation and not viability, however most triple combination pairs, most notably with Acetaldehyde, exposures resulted in cell death (**Figure 4.6 left**). Nicotine, in tertiary combinations had an overall decrease in viability,

and thereby differentiation (**Figure 4.6**). Benz(a)pyrene and Acetaldehyde alongside one of the other constituents still had significant decreases in differentiation, yet in comparison to the double combination calcium content was increased (**Figure 4.6**). Triple combinations containing Nicotine and Acrolein had overall no change to differentiation and a slight decrease in cell death compared to the double combination pair. The addition of the third chemical likely caused only a subtle effect on cellular health. Overall, it appears the addition of the third constituent Acrolein demonstrated the most disrupted effects to the combinations, in both directions. Triple combinations containing Acetaldehyde and Acrolein had an overall significant decrease in both calcium and viability, revealing three

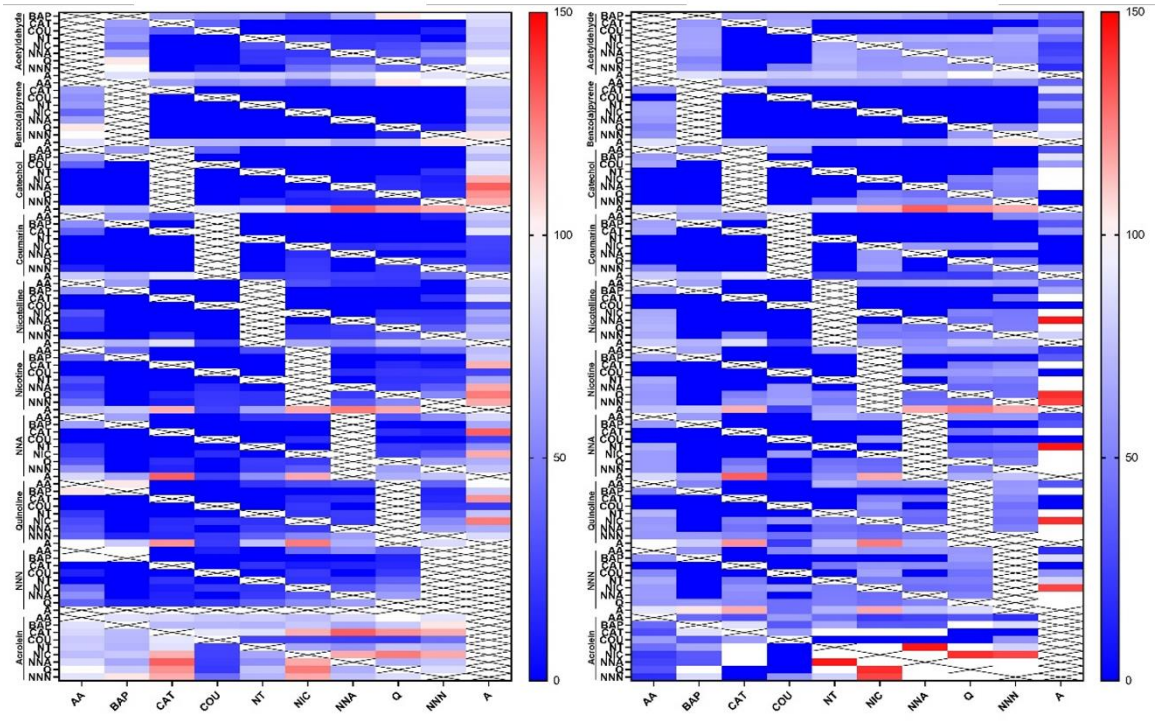

Figure 4.6 Triple Combination Heatmaps. MTT (left) and Calcium (right) assays corresponding to triple combinatorial exposures. Heatmaps were generated via GraphPad Prism. Data was normalized to Solvent Control (0.1% DMSO). AA = Acetaldehyde / BAP = Benzo(a)pyrene / CAT = Catechol / COU = Coumarin / NT = Nicotelline / NIC = Nicotine / NNA = 4-(methylnitrosamino)-1-(3-pyridyl)-1-butanone / Q = Quinoline / NNN = N-Nitrosonornicotine / A = Acrolein.

chemicals containing this combination results in cell death and therefore indirectly affecting differentiation.

The triple combination pair containing Catechol and Acrolein remains mostly unchanged despite differences in the third chemical. Interestingly, most of the triple combinations containing these two constituents appear to have an increased viability and differentiation in comparison to the double combination of this pair. The other 9 constituent combinatorial sets mostly mimicked effects seen in comparison to the double combinations. These ternary combinatorial data prove the unpredictable nature of toxicity when hundreds of thousands of constituents are present. However, it does appear that the combinatorial relationship could be further reduced to a single constituent provided a more intensive look of each constituent's mechanism of action was further evaluated.

4.4.3 *Total Combinatorial Exposure.* To further validate the synergistic combinatorial effect, the entire subset of constituents was tested to ultimately determine the effect on osteogenesis. Initially dosed at the individual ID_{50} concentrations, a total combination using the 10 chemicals was tested. Not surprisingly, at the ID_{50} concentration of the chemicals, cell viability showed a severely toxic response, and the differentiation counterpart was also significantly decreased (**Figure 4.7**). However, as the concentration of chemical actually found within tobacco is much lower than the identified ID_{50} concentrations, additional dilutions were next evaluated. Indeed, the cytotoxic effect lessened considerably with a 10-fold dilution (0.1x ID_{50}) and were almost negligible at the 100-fold dilution (0.001x ID_{50}). However, and more concerningly, the associated calcium data showed that even at the lowest concentrations of chemicals (0.001x ID_{50}) calcification

was still affected (**Figure 4.7 bottom**). With this work, the hypothesis that the full combination of chemicals found within tobacco smoke causes the hypomineralized phenotype appears to be true. Despite particular combination eliciting the differential effects, the addition of the third chemical and the total combination demonstrates that the full combinatorial effect explains the likely cause of the bone defect.

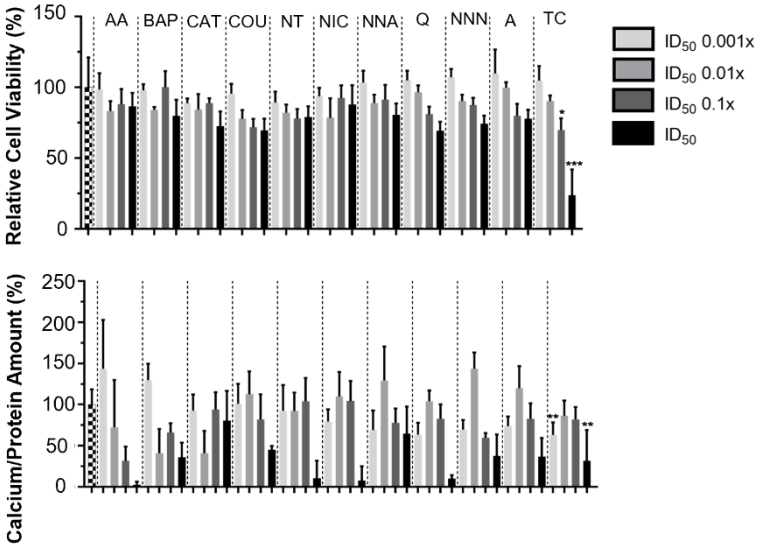

Figure 4.7 Total Combination Exposures. MTT (top) and Calcium (bottom) assays corresponding to single constituent and total constituent combinations. Data was normalized to Solvent Control (0.1% DMSO). AA = Acetaldehyde / BAP = Benzo(a)pyrene / CAT = Catechol / COU = Coumarin / NT = Nicotelline / NIC = Nicotine / NNA = 4-(methylnitrosamino)-1-(3-pyridyl)-1-butanone / Q = Quinoline / NNN = N-Nitrosonornicotine / A = Acrolein / TC = Total Combination

4.5 Discussion

Despite the Toxcast platform having access to over 11,000 chemicals and 21,000 assays, endpoints and gene targets related to osteogenesis were limited. Therefore, our output was based on *biological processes* to help predict cytotoxicity. The discrepancies between the ToxPI predictions and the *in vitro* data suggests an insensitivity of ToxPI teratogenic predictions. Despite the slight insensitivity, overall, this study effectively found that the ToxPI program, using the Toxcast database, can predictively isolate cytotoxic

constituents within tobacco smoke. This bodes exceptionally well for future studies that require the analysis of a concoction of constituents with unknown outcomes, such as those regularly encountered in agricultural and industrial settings. Moreover, despite the parameters chosen for the ToxPI analysis were not osteogenesis-specific, the ToxPI output was successfully extrapolated into our osteogenic protocol. Many of these constituents demonstrated skeletal-specific toxicity as demonstrated by lack of calcium content independent of cell death. Thereby, the ToxPI program, with collaboration with the Toxcast data proves to be a worthy database that has the potential to predictively detect maldevelopment within osteogenesis.

Although the ToxPI analysis did not identify nicotine as likely cytotoxic, this constituent was included due to prevalence in tobacco products and its highly addictive properties. Despite nicotine's noncytotoxic effect at lower concentrations, the constituent could still be contributing to the adverse effects on osteogenic differentiation. The ID_{50} value that was obtained for nicotine in the additional concentrations tested was 633.2 µg/mL. However, this concentration is relevant as the average concentration of nicotine found in the serum of chronic smokers is reported to be 33 ng/mL (Russell et al., 1980).

Aside from nicotine, we identified four HPHCs that elicited strong embryotoxic effects as indicated by relatively low concentrations required to inhibit differentiation. Most of these chemicals displayed embryotoxic effects independent of viability, however there are a few that indirectly affected differentiation due to cell death. In the dose-response generations, three of the predictive THS constituents (NAT, NFN, NNK) did not elicit an effect in cell viability or differentiation, which indicates absence of toxicity. Despite the

known carcinogenicity of tobacco-specific nitrosamines, the predicted THS constituents are potentially non-embryotoxic constituents. However, despite the increased ID_{50} concentration reported for THS constituents, combination analysis reveals an increase in cytotoxicity and a decrease in osteogenic yield. For instance, although seemingly harmless individually, NNK and NNN have been known to increase deleterious effects that can induce DNA double stranded breaks (Hang et al., 2013). In fact, in a related study, we found NNN may be a likely culprit behind osteogenic deficiency (Martinez et al., 2019).

Despite not further assessing null chemicals, aside from nicotine, constituents tested had variation in ID_{50} concentrations. In double combination work, we see nicotine (a null chemical) and Benz(a)pyrene (a known carcinogen) had a mild effect on both cytotoxicity and differentiation. However, the addition of any of the third chemicals resulting a drastic decrease in both viability and calcium content. Regardless of the individual dose-response curves demonstrating higher toxicity in some constituents, the combinatorial work shows the mixture effect. Further corroboration of these claims can be seen in our total combination exposure. Our data shows consistent dose-dependent responses in both viability and calcium content to individual constituents, yet the full concoction demonstrates an undeniable effect to differentiation.

Despite many particular combinations illustrating a significant effect solely on cytotoxicity and others on differentiation, no one *single* chemical could be pinpointed as the culprit of reduced calcification in response to tobacco exposure. These findings let us conclude that it may be difficult to isolate single chemicals as the primary drivers of embryotoxicity and that rather the full combination of chemicals in tobacco smoke may

produce the hypomineralization phenotype. These results have large implications beyond tobacco exposure, as many of the constituents screened can be routinely found in both public and industrial settings. The public is constantly being exposed to combinations of chemicals on a routine basis and now, we can peek into how these combinations may affect a sole aspect of human development. Future studies should be performed to determine potential synergistic effects of other developing models to gauge localized effects.

References

1. Acuff, L; Fristoe, K; Hamblen, J; Smith, M; Chen, J. 2016. Third-Hand Smoke: Old Smoke, New Concerns. *J Community Health.* 41:680–687. DOI 10.1007/s10900-015-0114-1

2. Berry, S. D., & Miller, R. R. 2008. Falls: epidemiology, pathophysiology, and relationship to fracture. *Current osteoporosis reports,* 6(4), 149–154. https://doi.org/10.1007/s11914-008-0026-4

3. Chen, YI., Chen, C. Lu, C. Tzeng, L. Tsao, J. Wang, 2003. Synthesis and anti-inflammatory evaluation of 9-phenoxyacridine and 4-phenoxyfuro[2,3-b]quinoline derivatives. Part 2, *Bioorg. Med. Chem.* 11:3921–3927.

4. Davis, L.A., Dienelt, A., zur Nieden, N.I., 2011. Absorption-based assays for the analysis of osteogenic and chondrogenic yield. Methods Mol. Biol. 690, 255–272.

5. Dienelt A; zur Nieden NI. 2011. Hyperglycemia impairs skeletogenesis from embryonic stem cells by affecting osteoblast and osteoclast differentiation. *Stem Cells Dev* 20(3):465-474.

6. ENVIRON International Corporation. Review of the Scientific Literature on Snus (Swedish Moist Snuff). *Environ.* 2013.

7. https://www.epa.gov/chemical-research/exploring-toxcast-data-downloadable-data

8. https://filtermag.org/fda-snus-harm-reduction/

9. Forte, AJ; Wilson, JM; Slattery, JT; Nelson, SD. 1984. The formation and toxicity of catechol metabolites of acetaminophen in mice. *Drug Metabolism and Disposition.* 12(4) 484-491

10. Genschow, E., Scholz, G., Brown, N., Piersma, A., Brady, M., Clemann, N., Huuskonen, H., Paillard, F., Bremer, S., Becker, K., Spielmann, H., 2000. Development of prediction models for three in vitro embryotoxicity tests in an ECVAM validation study. *In Vitr. Mol. Toxicol.* 13 (1), 51–66.

11. Genschow E; Spielmann, H; Scholz, G; Seiler, A; Brown, N; Piersma, A; Brady, M; Clemann, N; Huuskonen, H; Paillard, F; Bremer, S; Becker, K. (2002). The ECVAM international validation study on *in vitro* embryotoxicity tests: results of the definitive phase and evaluation of prediction models. *Altern. Lab Anim.* 30(2):151-76.

12. Hang, B., Sarker, A. H., Havel, C., Saha, S., Hazra, T. K., Schick, S., Jacob, P., 3rd, Rehan, V. K., Chenna, A., Sharan, D., Sleiman, M., Destaillats, H., & Gundel, L. A. 2013. Thirdhand smoke causes DNA damage in human cells. *Mutagenesis*, 28(4), 381–391. https://doi.org/10.1093/mutage/get013

13. Klingbeil, E. C., Hew, K. M., Nygaard, U. C., Nadeau, K. C. 2014. Polycyclic aromatic hydrocarbons, tobacco smoke, and epigenetic remodeling in asthma. *Immunol Res.* 58(0): 369–373. doi:10.1007/s12026-014-8508-1.

14. Knecht, AL; Goodale, BC; Truong, L; Simonich, MT; Swanson AJ; Matzke, MM; Anderson, KA; Waters, KM; Tanguay, RL. 2013. Comparative developmental toxicity of environmentally relevant oxygenated PAHs. *Toxicology and Applied Pharmacology.* 271: 266-275.

15. Lake, BG. 1999. Coumarin Metabolism, Toxicity and Carcinogenicity: Relevance for Human Risk Assessment. *Food and Chemical Toxicology.* 37: 423-453.

16. Laskar, A. A., Younus, H. 2019. Aldehyde toxicity and metabolism: the role of aldehyde dehydrogenases in detoxification, drug resistance and carcinogenesis, *Drug Metabolism Reviews,* 51:1, 42-64, DOI: 10.1080/03602532.2018.1555587

17. Martinez IKC, Sparks NRL, Madrid JV, Affeldt H 3rd, Vera MKM, Bhanu B, Zur Nieden NI. 2019. Video-based kinetic analysis of calcification in live osteogenic human embryonic stem cell cultures reveals the developmentally toxic effect of Snus tobacco extract. *Toxicol Appl Pharmacol.* 363:111-121. doi: 10.1016/j.taap.2018.11.006. Epub 2018 Nov 20. PMID: 30468815; PMCID: PMC6594699.

18. Moghe, A., Ghare, S., Lamoreau, B., Mohammad, M., Barve, S., McClain, C., Joshi-Barve, S. 2015. Molecular Mechanisms of Acrolein Toxicity: Relevance to Human Disease. *TOXICOLOGICAL SCIENCES*, 143(2), 242–255 doi: 10.1093/toxsci/kfu233

19. Nandhakumar, TR. Suresh, A.L. Calistus Judge, V.R. Kannan, P.S. Mohan. 2007. Synthesis, antimicrobial activities and cytogenetic studies of newer diazepino quinoline derivatives via Vilsmeier–Haack reaction, *Eur. J. Med. Chem*. 42:1128–1136.

20. Ratajczak, A.E.; Szymczak-Tomczak, A.; Rychter, A.M.; Zawada, A.; Dobrowolska, A.; Krela-Kazmierczak, I. 2021. Impact of Cigarette Smoking on the Risk of Osteoporosis in Inflammatory Bowel Diseases. *J. Clin. Med.* 10, 1515. https://doi.org/10.3390/jcm10071515

21. Reif, DM; Martin, MT; Tan, SW; Houck, KA; Judson, RS; Richard, AM; Knudsen, TB; Dix, DJ; Kavlock, RJ. 2010. Endocrine Profiling and Prioritization of Environmental Chemicals Using ToxCast Data. *Environ. Health Perspect.* 118(12): 1714–1720.

22. Russell MA, Jarvis M, Iyer R, Feyerabend C. 1980. Relation of nicotine yield of cigarettes to blood nicotine concentrations in smokers. *Br Med J.* 280(6219):972-6.

23. Scholz G, Genschow E, Pohl I, Bremer S, Paparella M, Raabe H, Southee J, Spielmann H (1999). Prevalidation of the Embryonic Stem Cell Test (EST)-A New *In Vitro* Embryotoxicity Test. Toxicol *In Vitro.* 13(4-5):675-81.

24. Sparks NRL; Martinez IKC; Soto CH; zur Nieden, NI. 2018. Low Osteogenic Yield in Human Pluripotent Stem Cells Associates with Differential Neural Crest Promoter Methylation. *Stem Cells*. 36(3):349-362.

25. Trettner S; Findeisen A; Taube S; Horn PA; Sasaki E; zur Nieden N.I. 2014. Osteogenic induction from marmoset embryonic stem cells cultured in feeder-dependent and feeder-independent conditions. *Osteoporos Int.* 25(4):1255-66.

26. US Food and Drug Administration. Harmful and Potentially Harmful Constituents in Tobacco Products and Tobacco Smoke: Established List. 2012. https://www.fda.gov/tobacco-products/rules-regulations-and-guidance/harmful-and-potentially-harmful-constituents-tobacco-products-and-tobacco-smoke-established-list

27. Walker, L., Baumgartner, L., Ast, J., Keller, K.C., Trettner, S., zur Nieden, N.I., 2014. Non-human primate and rodent embryonic stem cells are differentially sensitive to teratogens. *Tox. Reports* 2, 165–174.

28. Walker, L., Sparks, N., & Puig-Sanvicens, V., Rodrigues, B., zur Nieden, NI. 2021. An Evaluation of Human Induced Pluripotent Stem Cells to Test for Cardiac Developmental Toxicity. *International journal of molecular sciences.* 22. 10.3390/ijms22158114.

29. Xie, KZ. Chai, H. Piao, K. Kwak, Z. Quan. 2005. Synthesis and anticonvulsant activity of 7-alkoxyl-4,5-dihydro-[1,2,4]triazolo[4,3-a]quinolines, *Bioorg. Med. Chem. Lett.* 15:4803–4805.

30. zur Nieden NI; Kempka, G., and Ahr, H.J. 2003. *In vitro* differentiation of embryonic stem cells into mineralized osteoblasts. *Differentiation* 71:18-27.

31. zur Nieden, NI; Kempka, G; Ahr HJ. 2004. Molecular multiple endpoint embryonic stem cell test--a possible approach to test for the teratogenic potential of compounds. *Toxicol. Appl. Pharmacol.* 194(3):257-69.

32. zur Nieden, N.I., Davis, L.A., Rancourt, D.E., 2010. Comparing three novel endpoints for developmental osteotoxicity in the embryonic stem cell test. *Toxicol. Appl. Pharmacol.* 247 (2), 91–97.

33. zur Nieden, N.I., Baumgartner, L., 2010. Assessing developmental osteotoxicity of chlorides in the embryonic stem cell test. *Reprod. Toxicol.* 30(2), 277–283.

CHAPTER 5: RESCUE OF MINERALIZATION PHENOTYPE *IN VITRO* THROUGH SIGNAL MANIPULATION

5.1 Introduction

Mice exhibit skeletal defects in multiple bones and a distinct pattern of hypomineralization within a differentiating human *in vitro* model upon exposure to extracts of tobacco during early development. Our lab has attempted to flesh out chemical combinations that directly impact mineralization and produce the same phenotype as previously seen. In addition to this, an RNA-sequencing analysis was performed to determine key signaling dysregulations that could causally explain the phenotype seen both *in vivo* and *in vitro*. This is important, since any molecular insight can help elucidate key regulators that are perturbed in response to tobacco exposure.

Our prior work has found that multiple folate receptors are dysregulated due to embryonic tobacco exposure (**Figure 5.1**). This is not surprising, as folate deficiencies during embryonic development are known to cause neural tube defects. Additionally, in general, a folate deficiency can result in anemia and other associated symptoms. Therefore, an in depth investigation into folate regulation in a diseased system would help assess hypomineralization and other bone-related deformities associated with embryonic tobacco exposure. Although folate signaling is not involved directly in osteogenic differentiation, the one-carbon cycle is responsible for cellular metabolism and health. Folate acts as a carrier for one-carbon metabolism, which is factored into the synthesis of DNA and select amino acids. Additionally, folate is an antioxidant, and the one-carbon cycle plays a large role in antioxidant defense (Ducker and Rabinowitz, 2017). Therefore, even though folate

may not directly influence mineralization, dysregulation could explain the hypomineralization caused by tobacco exposure. Folic acid supplements are highly recommended to pregnant women to combat neural tube defects, which can be lethal to developing fetuses (Ducker and Rabinowitz, 2017). Bailey and Berry found depletion in mitochondrial folate directly led to neural tube defects and lethality (2005). In attempts to correct the folate deficiency, the defect was unable to be rescued (Bailey and Berry, 2005). This suggests that folate metabolism within the mitochondria is essential for one-carbon supplies for a developing embryo (Bailey and Berry, 2005). In embryonic development, the one-carbon cycle is mostly isolated to the mitochondria (Ducker and Rabinowitz, 2017).

Another notorious influencer to osteogenesis is *insulin* and *insulin-like growth factor* signaling. Insulin is most attributed to glucose mitigation, therefore can have substantial influence on embryonic development. In addition to implications *in utero, insulin* signaling is important for postnatal osteoblast and osteoclast production (Pramojanee et al., 2014). *Insulin-like growth factors* (*IGFs*) have some influence in embryonic skeletal development. *IGFs* have been shown to be expressed during limb morphogenesis (Agrogiannis et al., 2014). However, there are conflicting results that suggest *IGF* only plays a supportive role during skeletal development. Agrogiannis et al. found *IGF* knockout mice had impaired skeletal maturation, however no signs of limb dysplasia (Agrogiannis et al., 2014). Findings from this work could elucidate the role of that *insulin* and *IGFs* play during neural crest and paraxial mesoderm formation, and thereby bone development.

Follow-up validations to the previously collected RNA-sequencing work will provide novel insights into the molecular mechanism associated with perturbed osteogenic differentiation. My hypothesis is that amongst the identified dysregulations, folate and insulin signaling are likely the major dysregulators due to their highly integrated molecular mechanism. Manipulation of these receptors could rescue our mineralization phenotype. If this proves to be true, this work could lead to potential remedies in early-exposed embryos.

5.2 Previous Data

A global RNAseq experiment performed by the zur Nieden lab has identified many genes that are perturbed in response to Snus exposure (**Fig. 5.1A**). Differentiating H9 hESCs were lysed on day 7 of osteogenic differentiation and samples were submitted for RNA-sequencing. Sample groups included an untreated control, a non-effective dose of Snus (0.0005% PE), and an effective dose of Snus (0.1% PE) identified in a prior study

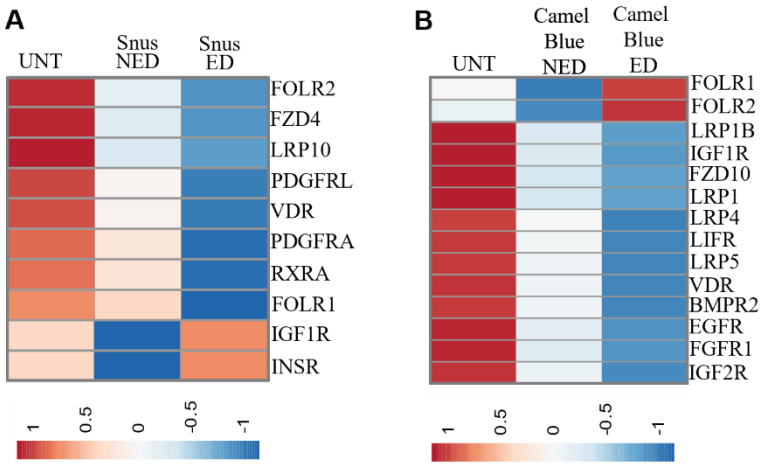

Figure 5.1 Heatmap comparing the deregulation of transcripts related to signals Total RNA from d7 samples, when the defect was already manifested, was extracted and libraries prepared using the NEBNext® Ultra™ II RNA Library Prep Kit from Illumina. Libraries were sequenced on the Illumina Nextseq 500 with an average of 38 mil reads/sample. Differential gene expression was calculated by DESeq2 with FDR < 0.05. The heatmaps were generated by normalizing the reads to RPKM and taking the average RPKM for each sample replicate (3 replicates per treatment). The z-score was calculated for the mean across all samples. **(A)** Snus receptor deregulations **(B)** Camel Blue receptor deregulations.

(Martinez et al., 2019). Differentially expressed genes (DEGs) were identified and shown to be associated with adversely affecting skeletal development. Among the DEGs, genes involved in fibroblast growth factors, folate receptors (*FOLR1*/*2*), WNT and BMP signaling pathways were enriched. More specifically, RNA-seq analysis revealed upregulation in insulin and insulin growth factor receptors (*INSR*/*IGFR*) and downregulation in folate receptors (*FOLR1*/*2*) (**Figure 5.1A**).

In addition to Camel Snus exposure being assessed in the global RNAseq experiment, the zur Nieden lab also identified many genes that are perturbed in response to Camel Blue exposure. Sample preparation, collection, and sequencing occurred as previously described. Sample groups included an untreated control, a non-effective dose of Camel Blue (0.0005 PE), and an effective dose of Camel Blue (0.14 PE) identifies in a previous study (Martinez et al., 2022). Camel Blue had similar signaling disruptions to Camel Snus, however there was differential regulation. RNA-seq analysis revealed downregulations in *INSR*/*IGFR* and upregulations in *FOLR1*/*2* (**Figure 5.1B**).

5.3 Methods

5.3.1 Cell Culture

H9 human embryonic stem cells (hESCs) were cultured on Matrigel (BD Biosciences) treated culture plates in mTeSR 1 medium (Stem Cell Technologies) at 37 °C with 5% CO_2. Colonies were passaged every 3 days using accutase (2–4 min at RT) and a cell scraper to displace colonies from the plastic well.

5.3.2 Osteogenic Differentiation of Human Embryonic Stem Cells

The differentiation protocol established and used within the zur Nieden lab uses confluent H9 hESCs to induce differentiation through the addition of a control differentiation medium (CDM) composed of DMEM, 15% FBS (Atlanta Biologicals), 1% (v/v) non-essential amino acids, 50 U/mL penicillin, 50 µg/mL streptomycin, and 0.1 mM β-mercaptoethanol. CDM is used for the first five days of differentiation to decrease pluripotency. On day five, CDM was supplemented with $1.2*10^{-7}$ M 1,25α$(OH)_2$ Vitamin D_3 (VD_3; Calbiochem), 0.1 mM β-glycerophosphate, and 20.8 µg/mL ascorbic acid. Additional supplements were curated and used to help cells further commit to osteoblast formation.

5.3.3 Tobacco Stocks Delivered During Osteogenic Differentiation

Extracts were made by incubating 10 g of Camel Snus in 100 ml of DMEM with 15% FBS overnight. The extract was centrifuged at 450 ×g for 10 min at room temperature and the supernatant again centrifuged at 13,000 ×g for 1 h to remove finer tobacco debris. The pH was adjusted to 7.4. Stocks were aliquoted and placed in -80°C to avoid freeze-thaw cycles and only removed when fresh medium was made.

5.3.4 Inhibitors and Mimics

IGF1R antibody (R&D systems; MAB391), Insulin (Sigma Aldrich; 11061-68-0), *FOLR1* antibody (R&D Systems; MAB5646), Folic Acid (Sigma Aldrich; 59-30-3), and PQ-401 (Sigma Aldrich; P0113) concentrations were selected based on previously reported IC_{50} values or established within the lab (https://www.abcam.com/pq-401-cell-permeable-igf1r-inhibitor-ab141077.html). Antibody and chemical stocks were reconstituted in 0.1%

BSA. Stocks were stored in -20 °C. Final dilutions were made in appropriate cell culture medium to the calculated ID_{50} concentration. Supplemental cell treatment started on either day 0 or day 5 of differentiation and continued through day 7 in H9 hESCs. Medium, including co-treatment dilutions, was made fresh and changed every other day.

5.3.5 Detection of Calcium

Quantification of calcium content was performed using a calcium assay normalized to protein content. Cells were lysed with radio-immunoprecipitation (RIPA) buffer (1% NP40, 0.5% sodium deoxycholate, 0.1% sodium dodecyl sulfate, PBS) on day 20 of cellular differentiation. Remaining matrix was washed with 1 N HCl and collected. Both lysates were assayed with Arsenazo III (Genzyme), and absorbance was measured at 655 nm (iMark microplate reader; BioRad). Absorbances were compared to a $CaCl_2$ standard and total calcium content was normalized to total protein content determined by a Lowry assay (Davis et al., 2011). Lowry assay was read at 750 nm (iMark microplate reader; BioRad) after a 15-minute micro-shake incubation and total protein was determined by comparing to a BSA standard curve.

5.3.6 Statistical Analysis

All exposures were performed in biological quintuplicates. In the following comparisons, co-treatments were compared to the relevant effective dose with a Welch's t-test via GraphPad Prism. A p-value below 0.05 was considered significant.

5.4 Results

5.4.1 *Camel Snus FOLR Signaling. FOLR1* and *FOLR2* were identified as notable transcript downregulations in the Snus effective dose. To validate the RNA-seq study and

take a first look into the causal relationship between Snus exposure and osteogenic defect, an effective dose of Snus was co-treated with the ligand, folate, which generally binds to both *FOLR1* and *FOLR2* (Chen et al., 2013).

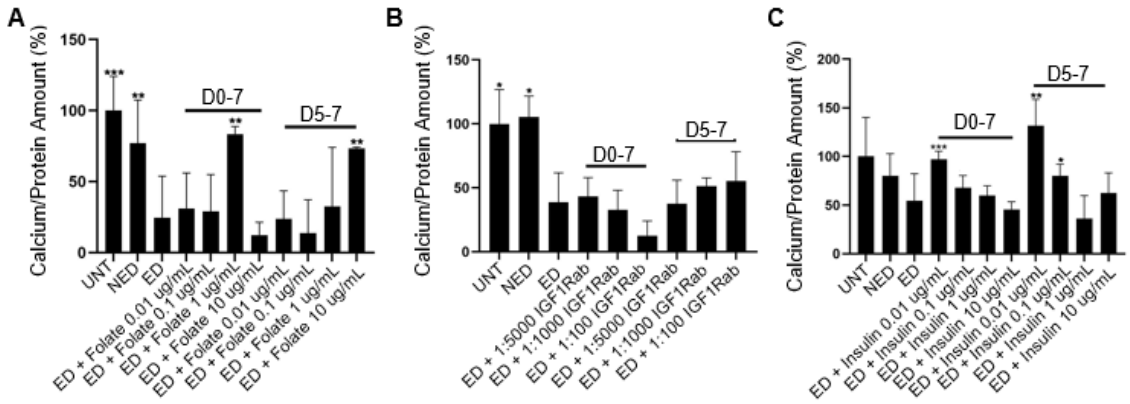

Figure 5.2. Snus co-treatments to assess receptor targets *FOLR1/2* and *IGF1R/INSR*. (A) Co-treatment with Folate rescued mineralization phenotype in ED, comparable to UNT. **p < 0.01; ***p < 0.001, n=5±SD, Welch's t-test. **(B)** Co-treatment of an *IGF1R* antibody with Snus did not significantly reduce calcium content. n=5±SD, Welch's t-test. **(C)** Co-treatment with insulin ligand in ED significantly rescued calcium phenotype. *p < 0.05; **p < 0.01; ***p < 0.001, n=5±SD, Welch's t-test. D = day / NED = non-effective dose / ED = effective dose.

Excess folate was expected to compensate for downregulation of receptor mRNA and rescue the osteogenic defect. Co-treatment was delivered at timepoints D0-7 and D5-7. Co-treatment timeframe day (D) 0-7 includes the entirety of early stem cell differentiation encompassing phases of gastrulation and specification into neural crest and mesoderm lineages. In contrast, during D5-7 cells are now moving into a mesenchymal stage, from which cells with pre-osteogenic properties are committed during the subsequent days. Both time windows have been previously shown to be sensitive to tobacco exposure, with days 5-7 being even more sensitive than d0-7 (Sparks et al., *Cell Biol Toxicol, in revision*). The calcification phenotype was significantly rescued in two instances of co-treatment. Specifically, there was a dose-dependency, as seen with

significant increase in calcium content at the highest folate dose (10 µg/mL) in both timepoints (D0-7 and D5-7) (**Figure 5.2C**).

5.4.2 *Camel Snus IGF1R Signaling.* As previously outlined, in Snus-treated differentiating hESCs, exposure resulted in an upregulation in insulin and insulin-like growth factor receptors (*INSR*/*IGFR*). To negate the resulting upregulation, cells exposed to an effective dose of Snus were co-treated with an *IGF1R* antibody, a selective inhibitor of *IGF1R* to reduce upregulation. Co-treatment with an *IGF1R* inhibitor should rescue the mineralization phenotype in Snus. However, co-treatment with an *IGF1R* antagonist resulted in no significant changes to mineralization content in comparison to the effective dose of Snus (**Figure 5.2B**). In fact, the highest concentration of *IGF1R* inhibitor in D0-7 demonstrated a decrease in percent of calcium, opposite to the expected.

Conversely, supplemental intake of insulin was also explored. Insulin can bind to both *IGF1R* and *INSR* (both upregulated receptors) as an agonist. This was followed based on the hypothesis that the increase in mRNA level may represent a feedback mechanism in response to non-responsive insulin signaling rather than represent a true increase. Indeed, osteogenesis was rescued in Camel Snus-treated hESCs when co-administered with insulin (**Figure 5.2C**).

5.4.3 *Camel Blue IGF1R Signaling.* RNA-seq data revealed *IGF1R* was downregulated in response to Camel Blue exposure, conversely of Camel Snus (**Figure 5.1**). Being that *IGF1R* is downregulated in the Camel Blue effective dose, supplemental co-treatment with insulin may be able to rescue the calcium phenotype. Indeed, this rescue was observed in all concentrations of d0-7 insulin co-treatment, with an optimal rescue noted at 0.1 µg/ml

of insulin (**Figure 5.3A**). While a rescue was also determined for the D5-7 exposure window, here, the rescue was only detected in the highest insulin concentration (10 µg/ml). Insulin concentrations were selected from previously identified ID_{50} concentrations. Next, a phenocopy experiment was conducted, in which hESCs were differentiated without Camel Blue exposure, but with increasing concentrations of PQ401, a selective IGF1R inhibitor. As expected, if tobacco exposure is to the detriment of osteogenesis due to inhibition of IGF1R, PQ401 supplementation concentration-dependently inhibited calcification output (**Figure 5.3B**).

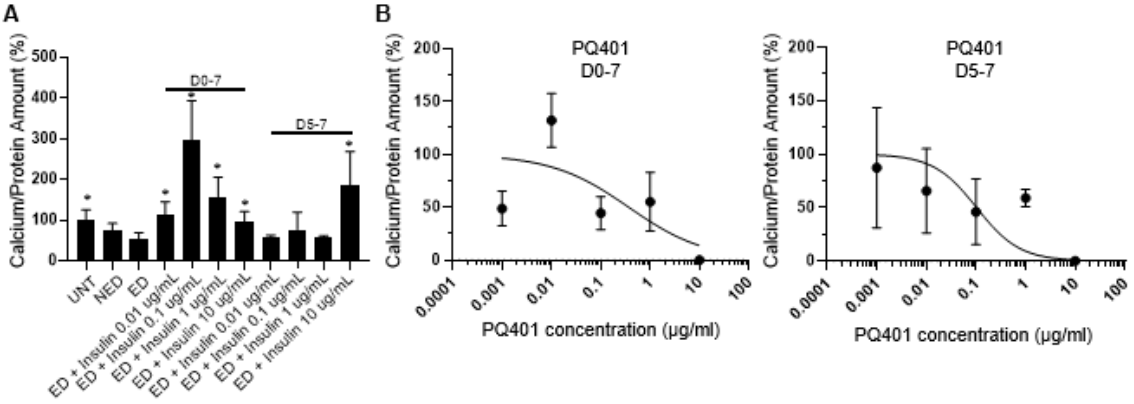

Figure 5.3 Camel Blue co-treatments to assess receptor targets IGF1R/INSR. A Welch's t-test was performed on each of the data sets compared to the ED using GraphPad Prism. (A) Supplemental human insulin (Sigma Aldrich; 11061-68-0) co-treatment was delivered days 0-7 or days 5-7. Co-treatment of insulin with Camel Blue significantly increased calcium content as expected, however with different effective concentrations depending on treatment time. *p < 0.5, n=5±SD, Welch's t-test. (B) Concentration-response curve for IGF1R inhibitor PQ401. Inhibitor treatment phenocopied the detrimental effect of Camel Blue in a concentration-dependent manner. D = day / UNT = untreated control / NED = non-effective dose / ED = effective dose

5.4.4 *Camel Blue FOLR Signaling.* Unlike in Snus-exposed cells, there was an upregulation in *FOLR* signaling in Camel Blue-exposed cells. A rescue experiment was performed to inhibit this upregulation of *FOLR1*. An effective dose of Camel Blue was co-treated with a *FOLR1* antibody, which selectively binds to *FOLR1* as an antagonist. Indeed,

there was a significant increase in the calcification phenotype in many instances of co-treatment (**Figure 5.4A**).

Similar to the phenocopy experiment above, a phenocopy experiment for folate was next designed. Again, osteogenically differentiating hESCs were supplemented with folate either during D0-7 or D5-7. If hypomineralization were through excel folate, a dose-dependent down-regulation of calcification was expected. This is indeed what was found for treatment window D0-7. However, in the second sensitivity window (D5-7) most concentrations of folate caused an increase in calcification, speaking to the beneficial effect of folate to differentiation, as also seen in the Camel Snus cultures (**Figure 5.4B**).

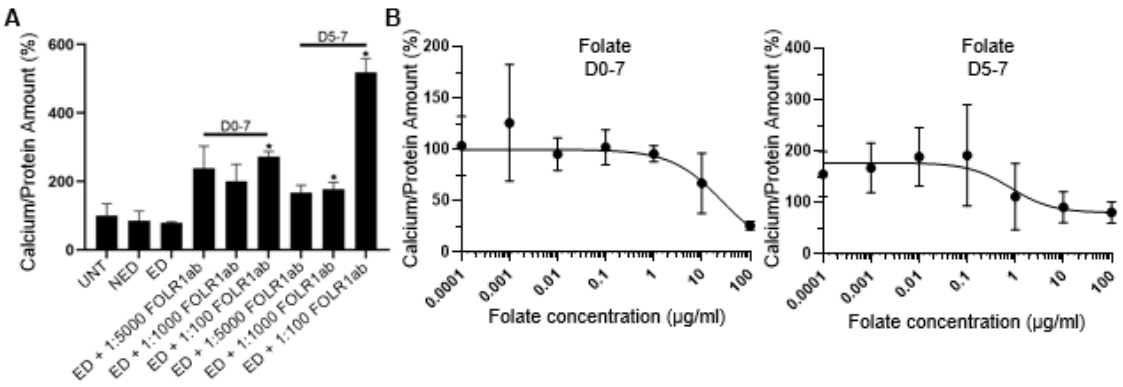

Figure 5.4 Camel Blue co-treatments to assess receptor target FOLR1. A Welch's t-test was performed on each of the data sets compared to the ED using GraphPad Prism. (A) Supplemental FOLR1 antibody (R&D Systems; MAB5646) co-treatment was delivered days 0-7 or days 5-7. Co-treatment with a FOLR1 antibody with Camel Snus significantly rescued calcification. *$p < 0.05$. (B) Concentration-response curve for folate. Folate exposure phenocopied the detrimental effect of Camel Blue in a concentration-dependent manner when exposure occurred in the first time window, but increased calcification in most concentrations when treatment happened from d5-7. D = day / UNT = untreated control / NED = non-effective dose / ED = effective dose

5.5 Discussion

The co-treatment timepoints are crucial especially in rescue cases as they delineate the brief period where exposure can be mitigated. Roughly around D7-8 is a timepoint when several cell types are committed that have the potential for subsequent osteogenesis,

including cells from neural crest and paraxial mesoderm lineages. Therefore, all lineages are influenced throughout the duration of the treatments described above. Although our model elucidates molecular alterations to osteogenesis during early development, remedial options remain available. Despite skeletal development and precursors to skeletal development occurring very early in embryonic development, initial OBGYN screenings should have onsite general curatives to negate any potential exposure. Remedies later in development post forelimb formation would prove to be slightly less effective. As detected by the discrepancies between the two co-treatment times, sensitivities related to timing of exposure corresponds to embryonic development.

Based on the inability to influence the calcium phenotype, it appears *IGFR* signaling is not contributing to the formation of the calcium matrix in the Snus treatments or, at the very least, *IGF1R* manipulation with the antibody is not enough to rescue the mineralization phenotype. In the case of Snus exposure, however, it does appear the resulting dysregulation of the osteogenic signaling pathway is highly influenced by folate signaling. This suggests there is a minimum excess folate needed to compensate for the receptor downregulation and *FOLR1* is important for the formation of the calcium extracellular matrix, as inhibition further depletes calcium content. As previously outlined, both *FOLR1/2* are downregulated in the Snus effective dose, and we hypothesized that the additional *FOL* ligand should compensate for the downregulation. This rescue was successfully performed, thus determining that folate has an influence on mineralization. Folate, itself, is a non-specific ligand that binds to both folate receptors, as well as contributes to the 1-carbon cycle in the production of nucleic acids (Ducker and

Rabinowitz, 2017). Despite our hypothesis to be true there was a seemingly dose and timing dependency of co-treatment. We found that the addition of folate significantly rescued calcification in some cases, despite reduced receptor signaling in the Snus effective dose. In the D0-7 timeframe the optimal concentration was identified to be 1 µg/ml of folate. In the higher 10 µg/ml co-treatment concentration of folate, a drop in calcium output was noted, which is likely attributed to overall cell death. As previously mentioned, folate is involved in other metabolic processes which could be altering both cellular health and mineralization. At the later timeframe (D5-7) of co-treatment, cultures are more robust at later stage of differentiation and can both survive and thrive from excess folate. Additionally, folate is a known anti-oxidant, therefore irregularities in anti-oxidant mechanisms can contribute to oxidative stress (OS) (Miller et al., 2008). This OS caused by perturbed folate function could explain the resulting phenotypes.

Unlike Snus, there was an upregulation in *FOLR* signaling of Camel Blue-exposed cells. While mineralization content was rescued with *FOLR1* antibody co-treatments, high concentrations were needed to offset the effects of Camel Blue exposure. The opposite directionality of regulation by the two tobacco products as well as the rescue and phenocopy experiments suggest that a particular level of folate signaling is necessary for proper differentiation progression and that deviation in any direction may lead to birth defects (Miller et al., 2008). This finding may have implications for the dosing of folate supplements taken by pregnant women, even in cases where there is no actual folate deficiency.

Within the Snus and insulin co-treatment, the addition of specific concentrations of insulin seemed to negate the exposure. Upon further investigation, it is speculated that this rescue may be due to the insulin-stimulated glucose transporter (Summers et al. 1998). Previous Western blots demonstrated that AKT2 (a relevant upstream target of FOXO) is downregulated in response to Camel Snus exposure. AKT2 is responsible for an AKT2-specific regulation of the trafficking of GLUT4, a glucose transporter. Therefore, with the reduced expression of AKT2, the Snus-exposed cultures may have reduced trafficking of GLUT4, thereby reducing glucose levels within the cell which can significantly alter cellular metabolism. However, with the excess treatment of insulin, the insulin-stimulated glucose transporter which is also mediated by GLUT4 can offset the effects seen by the AKT2 downregulation.

Overall, despite Camel Blue and Snus yielding similar phenotypes, it appears the hypomineralization is attributed to alternative signaling pathway regulation. The two cigarette smoke extracts seem to oppositely regulate folate and insulin signaling, however, both to the detriment of osteogenic differentiation efficiency. Previous work in our lab however, has shown that both tobacco products yield a reduction in the nuclear levels of the transcription factors FOXO1 and FOXO3a, concomitant with up-regulation of oxidative stress (Sparks, 2018 *dissertation*). It remains to be seen then, which of the receptors mediates this response in both treatment groups, which will be the subject of future work in the lab.

References

1. https://www.abcam.com/pq-401-cell-permeable-igf1r-inhibitor-ab141077.html

2. Agrogiannis, G.D., Sifakis, S., Patsouris, E.S., Konstantinidou, A.E. 2014. Insulin-like growth factors in embryonic and fetal growth and skeletal development (Review). *Molecular Medicine Reports,* 10, 579-584. https://doi.org/10.3892/mmr.2014.2258

3. Bailey, L.B., and Berry, R.J. (2005). Folic acid supplementation and the occurrence of congenital heart defects, orofacial clefts, multiple births, and miscarriage. *Am. J. Clin. Nutr.* 81, 1213S–1217S.

4. Chen C., Ke, J., Zhou, X. E., Wei Yi, W., Brunzelle, J. S., Jun Li, J., Yong, E., Eric Xu, H. E., Melcher, K. 2013. Structural basis for molecular recognition of folic acid by folate receptors. *Nature.* 500(7463): 486–489.

5. Davis, L.A., Dienelt, A., zur Nieden, N.I., 2011. Absorption-based assays for the analysis of osteogenic and chondrogenic yield. *Methods Mol. Biol.* 690, 255–272.

6. Ducker, G. S and Rabinowitz, J. D. (2017). One-Carbon Metabolism in Health and Disease. *Cell Metabolism.* 25: 27-42.

7. Martinez IKC, Sparks NRL, Madrid JV, Affeldt H 3rd, Vera MKM, Bhanu B, Zur Nieden NI. 2019. Video-based kinetic analysis of calcification in live osteogenic human embryonic stem cell cultures reveals the developmentally toxic effect of Snus tobacco extract. *Toxicol Appl Pharmacol.* 363:111-121. doi: 10.1016/j.taap.2018.11.006. Epub 2018 Nov 20. PMID: 30468815; PMCID: PMC6594699.

8. Miller JD, Chu Y, Brooks RM, Richenbacher WE, Pena-Silva R, Heistad DD. 2008. Dysregulation of antioxidant mechanisms contributes to increased oxidative stress in calcific aortic valvular stenosis in humans. *J Am Coll Cardiol.* 52(10):843–850

9. Pramojanee SN, Phimphilai M, Chattipakorn N, Chattipakorn SC. 2014. Possible roles of insulin signaling in osteoblasts. *Endocr Res.* 39(4):144-51. doi: 10.3109/07435800.2013.879168.

10. Sparks, NRL. 2018. The embryotoxic effects of harm reduction tobacco products on osteoblasts developing from human embryonic stem cells. *Dissertation.*

11. Sparks, N.R.; Madrid, J. V; Bottom, R; Vera-Colon, M. KM; zur Nieden, N. I. Differential predictivity of human pluripotent stem cell lines in skeletogenic developmental toxicity assays. *CRTOX*. In revision

12. Summers, S. A., Garza, L. A., Zhou, H., & Birnbaum, M. J. 1998. Regulation of insulin-stimulated glucose transporter GLUT4 translocation and Akt kinase activity by ceramide. *Molecular and cellular biology*, 18(9), 5457–5464. https://doi.org/10.1128/MCB.18.9.5457

CONCLUSION

This work outlined a highly reliable pipeline to assess developmental toxicants using a human-relevant approach. Additionally, some of the molecular mechanisms by which tobacco products may impact bone formation were uncovered. Follow-up experiments determined that the osteogenic differentiation pathway, while incredibly sensitive to embryo-toxicants, has room for remedial strategies.

The *in vivo* work highlighted, for the first time, discernable phenotypes associated with embryonic tobacco exposure. While no treatments were parlayed into the *in vivo* rodent work, the identification of specific bone-related phenotypes revealed components to development that are more sensitive to exposure over others. Paired with the *in vitro* technique and utilizing RNA-sequencing results, tobacco exposure was extensively assessed with real-life application.

There is some work remaining to further examine the ideas discussed here. Follow-up work should encompass other dysregulated signals perturbed due to Camel Blue and Snus exposure, as there was no definitive manipulation experiment that could causally relate Camel Blue AND Snus exposure to the previously observed FOXO attenuation (which causally relates to the osteogenic defect). In addition to follow-up *in vitro* signal manipulation, other bones, such as the full ribcage and the skull should be assessed to determine phenotypic changes that may arise in bones from the axial skeleton or such that are derived from a neural crest lineage. Indeed, preliminary image analysis of the 17.5 skulls detected porous bones in response to both exposures (zur Nieden lab, *unpublished*).

Overall, our hEST model has proven to be a reliable *in vitro* alterative to assessing bone development. Despite this work including an *in vivo* component, initial screenings were performed utilizing the *in vitro* differentiation protocol to identify the most harmful tobacco products to bone development, thereby reducing animals needed for screening. Additionally, the novel insight on influential effects to the molecular mechanism of tobacco-induced hypomineralization has greater implications in the realm of toxicology. This work provides a solid pathway to assess skeletal defects and coupled with the molecular insight could provide an avenue for human genetic screenings. This new understanding could be implemented by the American Academy of Pediatrics for pediatricians to conduct well-childcare exams in which pre-visit questionnaires include questions on the type of tobacco (or other relevant embryo-toxicants) the child was exposed to. Routine follow-up bone assessment should be performed to evaluate bone health and integrity and additional parental education pamphlets distributed to reduce fracture risk in the future.

APPENDIX

Chapter 2 Supplemental Figures:

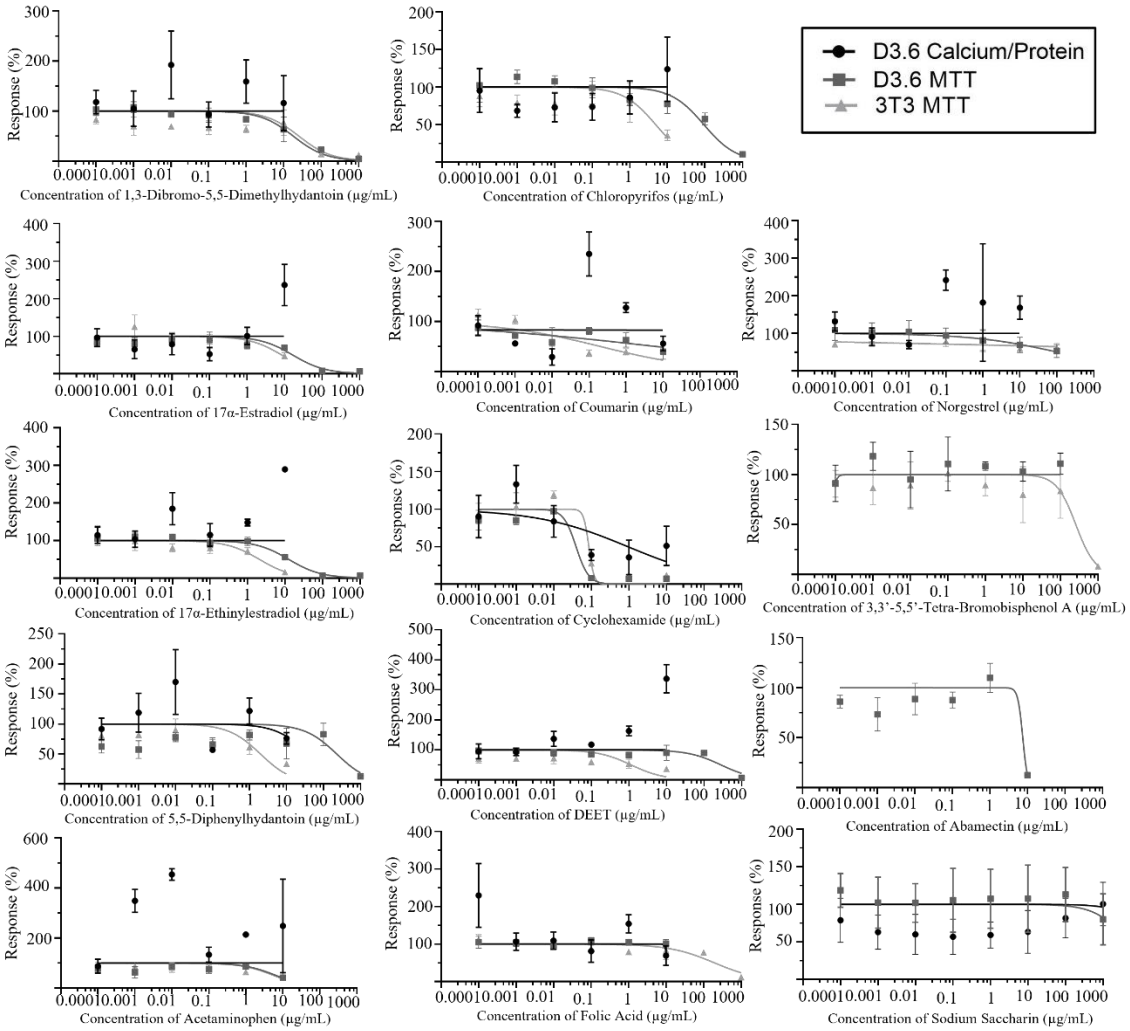

Supplemental Figure 2.1: Endpoint analysis was a calcium assay normalized to protein content (lowry) and 3-[4,5-dimethylthiazol-2yl]-2,5-diphenylterazolium bromide (MTT) assay (viability). Both endpoints occurred on day 20. Supplemental chemical exposure was delivered the entire duration of differentiation with the appropriate concentration. 3T3 mouse fibroblasts are a fully differentiated cell line with an endpoint of an MTT assay to quantify cell viability. Non-linear regression lines were fitted using GraphPad Prism to calculate ID_{50}/IC_{50} values.

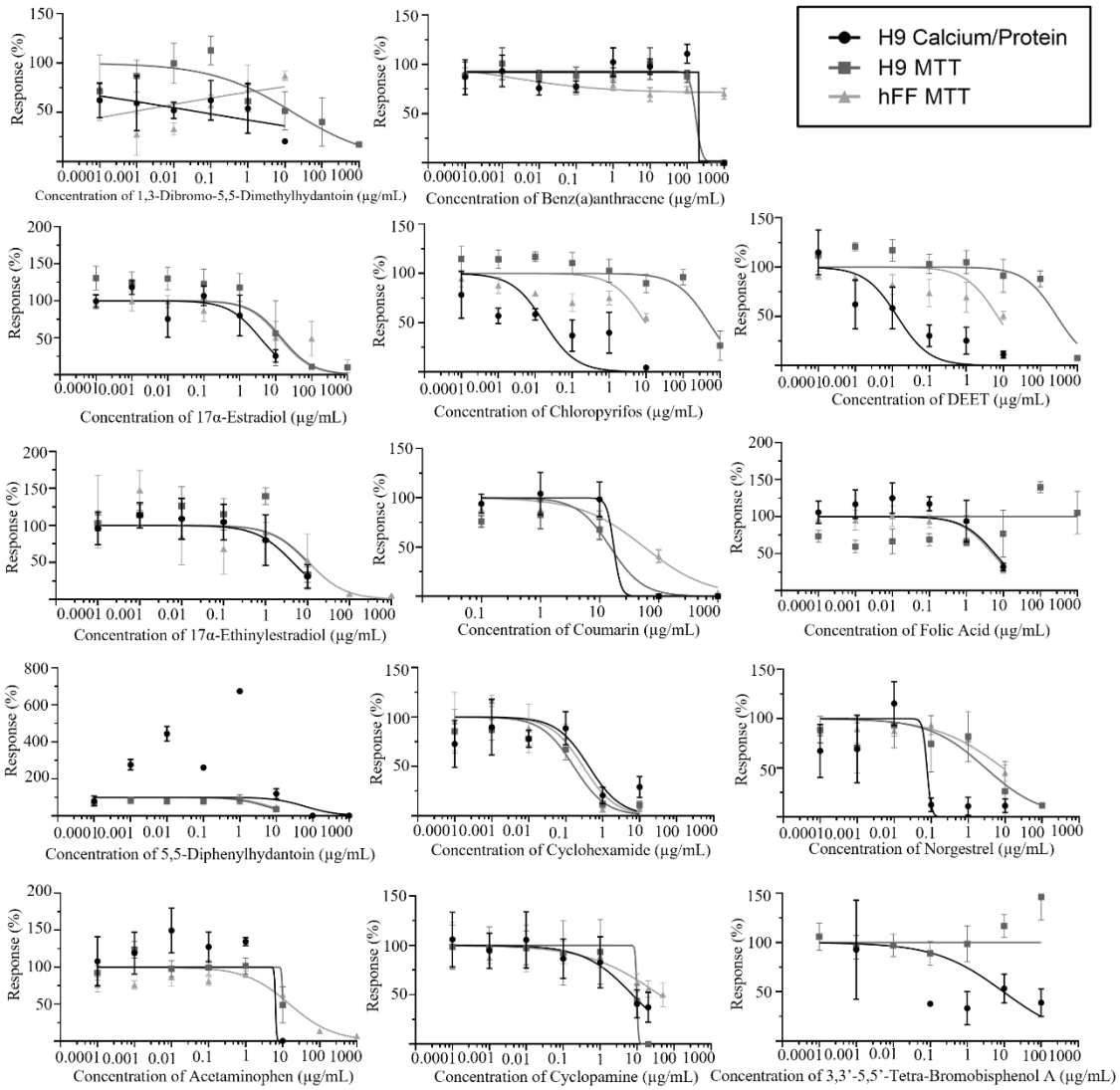

Supplemental Figure 2.2: Endpoint analysis was a calcium assay normalized to protein content (lowry) and 3-[4,5-dimethylthiazol-2yl]-2,5-diphenylterazolium bromide (MTT) assay (viability). Both endpoints occurred on day 20. Supplemental chemical exposure was delivered the entire duration of differentiation with the appropriate concentration. H9 hESCs were used at the human differentiating cell line. Human foreskin fibroblasts (hFF) are a fully differentiated cell line with an endpoint of an MTT assay to quantify cell viability. Non-linear regression lines were fitted using GraphPad Prism to calculate ID_{50}/IC_{50} values.

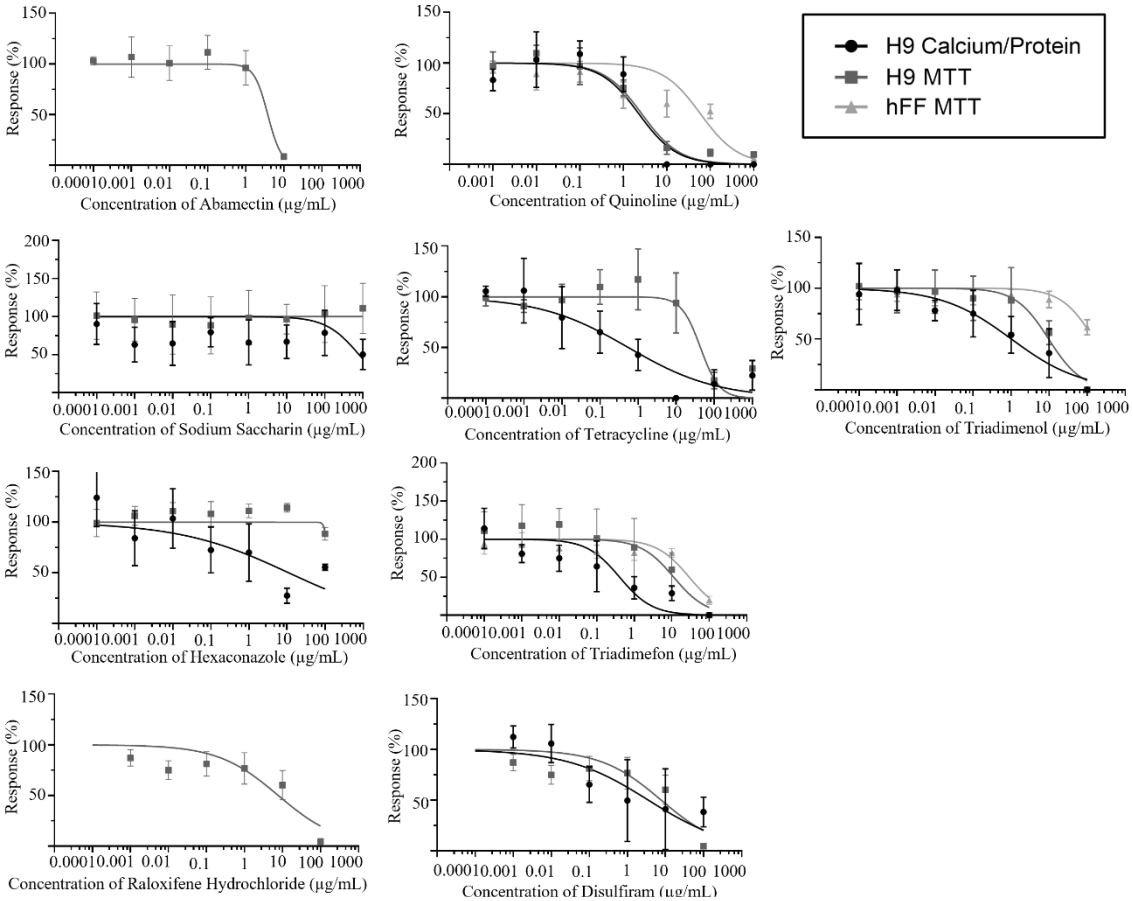

Supplemental Figure 2.3: Endpoint analysis was a calcium assay normalized to protein content (lowry) and 3-[4,5-dimethylthiazol-2yl]-2,5-diphenylterazolium bromide (MTT) assay (viability). Both endpoints occurred on day 20. Supplemental chemical exposure was delivered the entire duration of differentiation with the appropriate concentration. H9 hESCs were used at the human differentiating cell line. Human foreskin fibroblasts (hFF) are a fully differentiated cell line with an endpoint of an MTT assay to quantify cell viability. Non-linear regression lines were fitted using GraphPad Prism to calculate ID_{50}/IC_{50} values.